Aperture Neuro

Brook JBH, Salo T, Luo AC, et al. An open, fully-processed data resource for studying mood and sleep variability in the developing brain. *Aperture Neuro*. 2026;6(SI 1). doi:10.52294/001c.151820

Articles Describing Datasets

An open, fully-processed data resource for studying mood and sleep variability in the developing brain

Juliette B.H. Brook, B.A.[1,2,3†], Taylor Salo, Ph.D.[1,2,3†], Audrey C. Luo, B.S.[1,2,3], Joëlle Bagautdinova, M.S.[1,2,3], Sage Rush, M.S.E.d.[1,2,3], Aaron F. Alexander-Bloch, M.D., Ph.D.[1,3,4], Erica B. Baller, M.D., M.S.[1,2,3], Monica E. Calkins, Ph.D.[1,3], Matt Cieslak, Ph.D.[1,2,3], Elena C. Cooper, B.A.[1,3], John A. Detre, M.D.[5,6], Mark A. Elliott, Ph.D.[6], Damien A. Fair, Ph.D.[7,8,9], Phoebe Freedman, B.A.[1,3], Philip R. Gehrman, Ph.D.[1], Ruben C. Gur, Ph.D.[1,3,5,6], Raquel E. Gur, M.D., Ph.D.[1,3,4,5,6], Arno Klein, Ph.D.[10], Nina Laney, M.S.E.d.[1,3], Timothy O. Laumann, M.D., Ph.D.[11], Kahini Mehta, A.B.[1,2,3,12], Kathleen R. Merikangas, Ph.D.[13], Michael P. Milham, M.D., Ph.D.[10,14,15], Jonathan A. Mitchell, Ph.D.[16,17], Tyler M. Moore, Ph.D.[1,3], Steven M. Nelson, Ph.D.[8,9], Kosha Ruparel, M.S.E.[1], Brooke L. Sevchik, B.S.[1,2,3], Sheila Shanmugan, M.D., Ph.D.[1,3,6], Haochang Shou, Ph.D.[18,19], Manuel Taso, Ph.D.[20], Lauren K. White, Ph.D.[1,3], Daniel H. Wolf, M.D., Ph.D.[1,3,21], M. Dylan Tisdall, Ph.D.[5], David R. Roalf, Ph.D.[1,3], Theodore D. Satterthwaite, M.D.[1,2,3,5,21a]

[1] Department of Psychiatry, University of Pennsylvania, [2] Penn Lifespan Informatics and Neuroimaging Center (PennLINC), University of Pennsylvania, [3] Lifespan Brain Institute, Penn Medicine and Children's Hospital of Philadelphia, [4] Department of Child and Adolescent Psychiatry and Behavioral Science, Children's Hospital of Philadelphia, [5] Department of Neurology, University of Pennsylvania, [6] Department of Radiology, University of Pennsylvania, [7] Institute of Child Development, University of Minnesota, [8] Department of Pediatrics, University of Minnesota, [9] Masonic Institute for the Developing Brain, University of Minnesota, [10] Child Mind Institute, [11] Department of Psychiatry, Washington University in St. Louis, [12] Department of Neuroscience, Columbia University, [13] Genetic Epidemiology Research Branch, Intramural Research Program, National Institute of Mental Health, [14] Center for the Developing Brain, Child Mind Institute, [15] Nathan S. Kline Institute for Psychiatric Research, [16] Department of Pediatrics, University of Pennsylvania, [17] Division of Gastroenterology, Hepatology, and Nutrition, Children's Hospital of Philadelphia, [18] Center for AI and Data Science for Integrated Diagnostics (AI2D), University of Pennsylvania, [19] Penn Statistics in Imaging and Visualization Center, Department of Biostatistics, Epidemiology, & Informatics, University of Pennsylvania, [20] Siemens Medical Solutions USA Inc, [21] Center for Biomedical Image Computing and Analytics, University of Pennsylvania

Keywords: adolescence, development, fMRI, dMRI, ASL, EMA, actigraphy, emotion regulation, affective instability, sleep

https://doi.org/10.52294/001c.151820

Aperture Neuro

Vol. 6, Issue SI 1, 2026

Brain development during adolescence and early adulthood coincides with shifts in emotion regulation and sleep. Despite this co-occurrence, very few existing datasets simultaneously characterize affective dynamics, sleep variation, and multimodal measures of brain development. Here, we describe the study protocol and initial release (n = 10) of an open data resource of densely sampled behavioral measures and neuroimaging in adolescents and young adults. Behavioral measures include ecological momentary assessment, actigraphy, extensive cognitive assessments, and detailed clinical phenotyping focused on emotion regulation. All participants also complete multi-echo functional MRI, compressed-sensing diffusion MRI, and advanced arterial spin-labeled MRI. All raw and processed data are openly available without a data use agreement and will be regularly updated as accrual continues. Together, this resource will accelerate research on the links between mood, sleep, and brain development.

INTRODUCTION

Affective instability is characterized by frequent mood shifts and disturbances in emotional intensity,[1] similar to constructs such as mood instability and emotional dysregulation.[2] Affective instability is present in multiple psychiatric disorders, including borderline personality disorder (BPD), attention-deficit hyperactivity disorder (ADHD), post-traumatic stress disorder (PTSD), and major depressive disorder (MDD).[3] Typically emerging when youth learn to self-regulate changes in their affective states or mood,[1] affective instability has been associated with suicidality and suicide attempts.[4] Despite increasing rates of mental disorders and suicide in youth,[5] the neurodevelopmental underpinnings of affective instability remain sparsely studied and poorly understood.[6] Here, we describe the study protocol and first data release of a new open data resource focused on brain development, affective instability, and sleep.

† Joint first authors

a Corresponding Author:
Theodore D. Satterthwaite
sattertt@pennmedicine.upenn.edu

Adolescence represents an important period for investigating changes in emotion regulation, as developmental changes in the capacity for emotion regulation occur during adolescence.[7] Compared to adults, emotional reappraisal in adolescence is shorter and less salient – adults are more successfully able to reframe their perception of stimuli in order to alter its emotional impact.[8] As a result, successful cognitive reappraisal of events improves with age,[9] with age-related improvements in emotion regulation being related to changes in prefrontal-amygdala circuitry.[10,11] The onset of many neuropsychiatric disorders that involve affective instability occurs during adolescence such as ADHD, anxiety, and substance use disorders.[12] Adolescence and young adulthood thus represent an important age window to study brain development and risk for mental illness.

Affective instability is challenging to measure. Affective instability is a trait-like construct,[13] whereas emotion regulation refers to a skill or process in which individuals influence how they experience and express their emotions.[14] While there are numerous self-report scales (e.g., Affective Control Scale,[15] Difficulties in Emotion Regulation Scale,[16] etc.) and semi-structured interviews (e.g., Emotion Regulation Interview,[14] Structured Clinical Interview for DSM-5 Axis II Personality Disorders,[17] etc.) that assess aspects of affective instability, their retrospective nature limits accuracy and can be susceptible to memory distortion.[18] Ecological momentary assessment (EMA) offers a promising alternative by measuring participants' self-reported symptoms and activities as they occur in daily life, providing contextual richness and naturalistic data.[19] EMA can identify the temporal dynamics of adolescent emotion regulation across unique contexts. Past studies have leveraged EMA in adolescents to identify moment-to-moment affective changes related to adolescent-parent interactions[20] as well as time-related changes and gender differences in anxiety symptoms (e.g., anticipatory worry, negative expectations).[21] These strengths have led to the increased use of EMA in studies of BPD,[22,23] MDD,[20] and other related disorders in childhood.[21]

Sleep quality is closely tied to affective dynamics and emotion regulation in youth. Substantial evidence indicates that sleep disruption (e.g., sleep deprivation, insomnia) drives emotion dysregulation and predicts the onset of mood disorders in adolescence.[24-29] Additionally, sleep is thought to be linked to critical plasticity mechanisms of healthy brain development,[30-33] with impaired sleep contributing to variation in brain structure and function.[34-40] Daytime physical activity has also been associated with affective dynamics, where lower levels of physical activity tend to worsen emotion regulation and mood.[41,42] While sleep and physical activity are often assessed with parent or self-report questionnaires, research-grade actigraphy recordings provide sensor-based data that overcome questionnaire-related limitations of recall bias. Actigraphy tracks sleep and physical activity for up to several weeks in real-world settings, providing a unique opportunity to collect more accurate, dense, and ecologically valid measures of a person's lifestyle.[43-45]

Neuroimaging data can be integrated with the high-quality behavioral measures described above to further characterize the neurodevelopmental underpinnings of affective dynamics. However, recent evidence suggests that due to small effect sizes, large samples are necessary to uncover generalizable brain-behavior relationships, posing a significant methodological challenge to understanding how variation in brain development connects to affective instability and mood dysregulation.[46,47] Small effect sizes observed may be due, in part, to poor reliability and inaccurate measurements of key behavioral phenotypes,[46,48,49] un-modeled individual variation in neuroimaging measures,[50,51] and biological heterogeneity.[52-54] However, studies can improve signal and minimize noise by collecting precise individualized measures of behavioral and brain data.[51] The recent advent of multi-echo functional MRI (ME-fMRI)[55,56] and other enhanced imaging sequences (like compressed sensing diffusion spectrum imaging; CS-DSI)[57] may allow for identification of person-specific variation with less data.[55] For example, previous research has demonstrated that 10 minutes of ME-fMRI data produced more reliable estimates of functional connectivity than 30 minutes of single-echo (SE) fMRI in the cortex, cerebellum, and subcortical structures.[55] Thus, pairing contemporary EMA and actigraphy procedures that densely sample mood and sleep with more precise imaging methods may hold promise for linking variation in affective dynamics to brain development in youth.

In this paper, we describe the protocol and initial data release from a new study that leverages recent advances in characterizing complex behavior and non-invasive brain imaging to investigate affective instability in youth. Specifically, we employ a combination of EMA techniques and specialized self-report scales to assess affective instability and emotion regulation. Furthermore, the study measures sleep via wearable actigraphy devices in addition to EMA and other self-report measures. Perhaps most importantly, the study includes advanced imaging methods – such as ME-fMRI, CS-DSI, and advanced arterial spin-labeled (ASL) perfusion MRI – to characterize structural and functional brain development. Notably, both raw and processed data are fully de-identified and openly shared without a data use agreement. This small study is designed as an open data resource that combines multiple data types of interest. We anticipate that this data resource will assist researchers in designing larger studies and in developing new methods. Furthermore, we expect that this data resource will accelerate translational research on affective instability in youth.

METHODS

PARTICIPANTS

This study aims to recruit 100 individuals between the ages of 13 and 23. Participants must be proficient in English, able to understand the study procedures, and agree to participate by giving written informed consent or assent. Exclusion criteria include any significant medical or neurological illness that may impact brain function or a history

of pervasive developmental disorder, psychosis, bipolar disorder, or clinically significant current substance misuse. Furthermore, participants who present with acute intoxication with alcohol or other substances or lack a mobile device with capabilities to complete the study procedures are excluded. Additional exclusion criteria include pregnancy, implanted ferrous metal, claustrophobia, and other contraindications to MRI. Initial recruitment was focused on young adults as study procedures were being finalized; the initial data release includes 10 participants (mean age = 21.5, SD = 1.33; M:F 4:6). Recruitment is ongoing to reach the full sample size of 100 participants.

Participants are primarily recruited through medical record review at the Children's Hospital of Pennsylvania (CHOP) and Penn Medicine. In addition, individuals who had previously participated in research within the Department of Psychiatry may be recontacted to participate in the current study. Other recruitment strategies include physician referrals within the Penn Medicine and CHOP systems, announcements on the lab website, and advertisements around Philadelphia. All study procedures are approved by the Institutional Review Boards of both the University of Pennsylvania and CHOP; all participants provide written informed consent. For participants under the age of 18, a parent or legal guardian provides informed consent and the minor provides informed assent.

BEHAVIORAL AND CLINICAL ASSESSMENTS

This study includes an array of assessments. These include self-report measures, clinical assessments, a cognitive battery, mobile phenotyping with EMA, actigraphy via a wearable wristwatch-like device, and MRI. Figure 1 presents the study timeline of assessments. First, the study team identifies and recruits participants through a phone call screener. Second, participants complete the in-person imaging visit at the Hospital of the University of Pennsylvania. The cognitive assessments are administered on the same day as the in-person imaging visit. Participants begin the EMA and actigraphy procedures within 24 hours of the imaging visit. Participants are provided the actigraphy device fully charged as well as a prepaid shipping envelope to return the device after three weeks. Participants also complete a remote clinical assessment session within the same week of the imaging visit.

SELF-REPORT SCALES

A series of self-report scales assess demographic information, local environment, sleep, emotion regulation, and other domains of mental health. Table 1 presents the self-report questionnaire battery administered during the remote clinical assessment visit.

PUBERTAL MEASURES

Participants under the age of 18 complete the Self-Administered Instrument to Assess Stage of Adolescent Development,[58] that uses Tanner's images[59] to determine pubertal status in adolescent populations. The scale has been previously used in other studies investigating adolescent brain development.[60-62] Male and female participants receive distinct versions of the scale. Both versions are seven items and include two items where participants indicate how their development compares to Tanner's images; the items differ between male and female versions asking either about male pubertal changes (e.g., facial hair growth, deepening voice, etc.) or female pubertal changes (e.g., menstruation).

MEASURES OF THE CHILDHOOD ENVIRONMENT

Five scales assess childhood environment. First, the Childhood and Adolescent Trauma Screen (CATS)[63] is a self-report questionnaire that examines participants' exposure to potentially traumatic events (PTEs) and post-traumatic stress symptoms. An abbreviated 9-item version includes a structured PTE checklist asking about traumatic events (e.g., natural disasters, accidents, etc.) reflected in the DSM-5 criteria for PTSD. Furthermore, participants complete the Neighborhood Safety and Crime Short-Form (NSC; 3-item questionnaire)[64] and the Neighborhood Community Cohesion Short-Form (NCC; 5-item questionnaire),[64] two brief self-report scales that address neighborhood socioeconomic position. Finally, the Accountable Health Communities Health-Related Social Needs Screening Tool (AHC-HRSN)[65] is a 14-item self-report scale that screens for non-medical health-related needs in the following domains: housing instability, food insecurity, transportation difficulties, utility assistance needs, interpersonal safety, financial strain, family and community support, education, physical activity, and disabilities. An additional 12 items are asked to obtain demographic and socioeconomic information from participants related to income, education, and household factors.

SELF-REPORT SLEEP MEASURES

Three scales assess sleep. First, the Sleep Reduction Screening Questionnaire (SRSQ)[66] is a 9-item self-report questionnaire measuring individual sleep need through daytime symptoms and interrogating sleep problems in order to assess perceived symptoms of sleep reduction (e.g., insufficient/poor sleep). Second, the Ultra-Short Munich ChronoType Questionnaire (uMCTQ)[67] is a 6-item self-report questionnaire designed to evaluate sleep-wake behavior. Finally, the PROMIS Pediatric Sleep Disturbance Short Form (PROMIS SD Short Form 4a)[68] is a 4-item self-report measure evaluating sleep and wake function.

MEASURES OF EMOTION LABILITY, REACTIVITY, AND REGULATION

All participants complete an extensive battery including five complementary measures related to emotion regulation. First, the current study uses an abbreviated 5-item version of the Difficulties in Emotion Regulation Scale (DERS)[16] assessing clinically relevant difficulties in emotion regulation. Second, the Emotion Regulation Questionnaire-Short Form (ERQ-S)[69] is a 6-item self-report scale assessing two distinct emotion regulation strategies: cognitive reappraisal and expression suppression, designed for time-pressured settings. Third, the Affective Reactivity Index (ARI)[70] is a 7-item self-report questionnaire that eval-

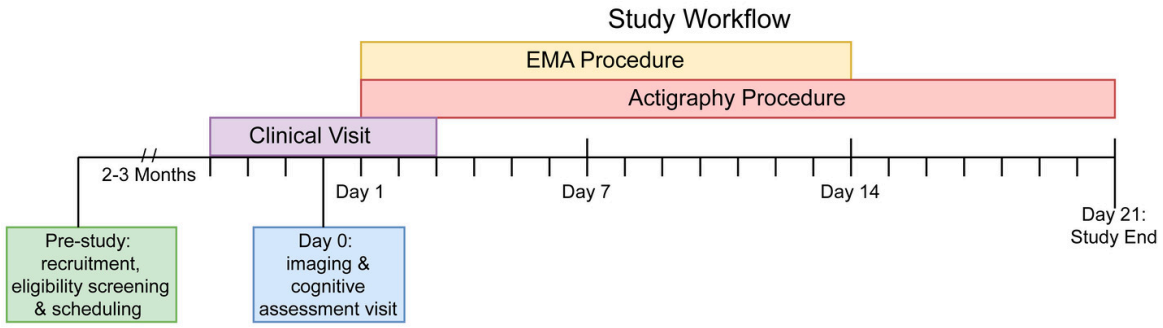

Figure 1. Study timeline.

uates irritability over the past six months, focusing on feelings and behaviors specifically relevant to irritability, as well as overall impairment due to irritability. Fourth, the Extended Strengths and Weaknesses Assessment of DMDD Symptoms and Normal Behavior (E-SWAN DMDD)[71] is a 30-item self-report questionnaire that measures elements of disruptive mood dysregulation disorder (DMDD). Fifth, participants complete a 10-item version of the Borderline Evaluation of Severity over Time (BEST)[72] scale which measures symptoms of BPD, including the Thoughts and Feelings (e.g., changes in self-identity, feelings of emptiness, etc.) and Behaviors-Negative (e.g., self-injury, impulsive sexual behavior, etc.) subscales. Sixth, participants complete the 5-item Reward Responsiveness subscale of the Behavioral Inhibition System and Behavioral Activation System Scales (BIS/BAS).[73]

ADDITIONAL CLINICAL SELF-REPORT MEASURES

In addition to detailed measures of emotion regulation, the study collects data on stressful life events, the symptoms of major depressive disorder (MDD), attention-deficit hyperactivity disorder (ADHD), and subthreshold symptoms of psychosis in three assessments. First, the Perceived Stress Scale-4 (PSS-4)[74] is a 4-item self-report measure that assesses the degree of appraised stress associated with life events over the last month. Second, the Patient Health Questionnaire (PHQ-8)[75] is an 8-item self-report measure of depression. Derived from the PHQ-9,[76] the PHQ-8 includes all equivalent items except for item 9, which addresses thoughts of death or self-harm. Of note, item 9 was not administered due to issues of monitoring self-harm virtually. Third, the Extended Strengths and Weaknesses Assessment of ADHD Symptoms and Normal Behavior (E-SWAN ADHD)[71] is an 18-item self-report questionnaire that measures ADHD. Lastly, the PRIME Screen Revised 5-item (PRIME-5)[77] is a brief self-report measure that serves as an age-normed subthreshold psychosis screening tool.

STRUCTURED ASSESSMENT OF CLINICAL DOMAINS

Participants complete the Computerized Adaptive Testing (CAT) GOASSESS[78] psychopathology screener. The CAT GOASSESS is an adapted version of the highly-structured GOASSESS screening interview,[61] and includes five domains: mood/anxiety, phobias, externalizing, psychosis, and pathological personality characteristics. While the full GOASSESS takes an hour on average to administer, the CAT GOASSESS is designed for rapid administration – often requiring only minutes – and minimal proctoring.[78] Table 2 compares the interview sections captured within the full and CAT GOASSESS versions.

COGNITIVE BATTERY

We measure cognition using the Penn Computerized Neurocognitive Battery (CNB).[79] The CNB contains a series of computerized tests that are administered by a member of the research team. Participants typically complete the entire battery within an hour. The CNB evaluates performance accuracy and speed on neurobehavioral domains including: executive control, episodic memory, complex cognition, social cognition, sensorimotor speed, and reward decision-making.[80] The CNB tests used in this study include the Abstraction, Inhibition, and Working Memory Test, Psychomotor Vigilance Test (3 Minute Version), Short Penn Continuous Performance Task (Adaptive), Digit Symbol Test, Penn Trailmaking Test (B Version), Short Letter-N-Back Test (2 Back Version), Short Visual Object Learning Test, Short Penn Logical Reasoning Test, Penn Emotion Recognition Task, and the Motor Praxis Test.

In addition to the CNB tasks described above, participants complete further cognitive assessments that use computerized adaptive testing (CAT) versions of the CNB. The CAT-CCNB evaluates the same domains, adding two measures of complex cognition (the Penn Matrix Analysis Test and the Penn Line Orientation Test), another measure of social cognition (the Measured Emotion Differentiation Test), and two reward/decision-making tests (Delay Discounting and Risk Discounting).[81] Table 3 details the complete battery of cognitive tests and relevant domains.

ECOLOGICAL MOMENTARY ASSESSMENT

Following the in-person imaging visit, participants begin a 2-week EMA procedure with a mobile app entitled the "Real-time Ecological Assessment of the Context of mental and physical Health (*REACH*)," developed through a collaborative effort between the NIMH Intramural Research Program and the Child Mind Institute, adapted on the Curious

Table 1. Self-report scales.

Scale Administered	Short Name	Outcome Assessed	Reference
Difficulties in Emotion Regulation Scale	DERS	Emotion Regulation	Gratz & Roemer (2004)
Affective Reactivity Index	ARI	Irritability	Stringaris et al. (2012)
Borderline Evaluation of Severity over Time	BEST	Borderline Personality Disorder	Pfohl et al. (2009)
Extended Strengths and Weaknesses Assessment of DMDD Symptoms and Normal Behavior	E-SWAN DMDD	Disruptive Mood Dysregulation Disorder	Alexander et al. (2020)
Sleep Reduction Screening Questionnaire	SRSQ	Sleep Reduction	van Maanen et al. (2014)
Ultra-Short Munich ChronoType Questionnaire	uMCTQ	Sleep-wake Behavior	Ghotbi et al. (2020)
Emotion Regulation Questionnaire - Short Form	ERQ-S	Emotion Regulation, Cognitive Reappraisal, Expressive Suppression	Preece et al. (2023)
Patient Health Questionnaire 8-item	PHQ-8	Depression	Kroenke et al. (2009)
Extended Strengths and Weaknesses Assessment of ADHD Symptoms and Normal Behavior	E-SWAN ADHD	Attention-deficit/Hyperactivity Disorder	Alexander et al. (2017)
PROMIS Pediatric Sleep Disturbance [Short Form 4a]	PROMIS SD	Sleep Disturbance, Sleep and Wake Function	Yu et al. (2012)
PRIME Screen Revised 5-item	PRIME-5	Early Subthreshold Psychosis Symptoms	Calkins (2025)
Behavioral Inhibition/Activation System Reward Subscale Child	BIS/BAS Reward Child	Motivational Systems	Carver & White (1994)
Pubertal Development Scale [Male]	PDS-Tanner-M	Male Adolescent Development	Morris & Udry (1980)
Pubertal Development Scale [Female]	PDS-Tanner-F	Female Adolescent Development	Morris & Udry (1980)
Perceived Stress Scale-4	PSS-4	Nonspecific Appraised Stress	Cohen et al. (1983)
Child and Adolescent Trauma Screen	CATS	Posttraumatic Stress Symptoms	Sachser et al. (2017)
Neighborhood Safety and Crime Short-Form	NSC	Residential Environment, Socioeconomic Position	Mujahid et al. (2007)
Neighborhood Community Cohesion Short-Form	NCC	Residential Environment, Socioeconomic Position	Mujahid et al. (2007)
Accountable Health Communities Health-Related Social Needs Screening Tool	AHC-HRSN	Housing Instability, Food Insecurity, Exposure to Interpersonal Violence	Billioux et al. (2017)

(formerly: MindLogger) Platform.[82] Curious allows studies to design mental health assessments and interventions that are distributed to participants through customizable mobile or web activities.

EMA assesses participants' emotions at the time of sampling rather than gathering a retrospective report on how they felt over the past week or month. Computerized EMA allows studies to verify the exact time when survey responses occurred[83]; it thus reduces retrospective bias, provides real-time tracking of dynamic processes, and contextualizes relationships between symptoms and behaviors.[82] *REACH* emerged after more than a decade of development and expansion of ecological assessment of emotional states with the mood circumplex[84] as well as correlates of mood including sleep, physical activity, and energy.[85] *REACH* includes modules on the mood circumplex, negative thoughts, sleep, context, screen and social media usage, life events, physical activity, food and drink intake, pain,

Table 2. GOASSESS structured clinical interview.

Interview Component	Full GOASSESS	CAT GOASSESS
Timeline	✓	
Demographics and Medical History	✓	
Psychopathology Screener		
Anxiety	✓	
Generalized Anxiety	✓	
Separation Anxiety	✓	
Specific Phobia	✓	✓
Social Anxiety	✓	✓
Panic	✓	✓
Agoraphobia	✓	✓
Obsessive-Compulsive	✓	✓
Post-traumatic Stress	✓	✓
Mood	✓	✓
Major Depression	✓	✓
Mania/Hypomania	✓	✓
Behavioral	✓	✓
Attention Deficit/Hyperactivity	✓	✓
Oppositional Defiant	✓	✓
Conduct	✓	✓
Psychosis	✓	✓
Psychosis	✓	✓
Prodromal Screen (PRIME/SIPS)	✓	✓
Eating	✓	✓
Anorexia	✓	✓
Bulimia	✓	
Other	✓	
Treatment History	✓	
Suicide	✓	
Substance		
Other Disorders		
Child Global Assessment of Function	✓	
Personality Interview for DSM-5 Brief Form	✓	✓
Interviewer Observations	✓	

Elements of the Full and CAT versions of the GOASSESS are detailed.

Table 3. Cognitive battery domains.

Test	Domain	Adaptive Design
Motor Praxis Test	Sensorimotor speed	
Penn Emotion Recognition Task	Emotion recognition	
Abstraction, Inhibition, and Memory Test	Executive Function	
Short Penn Logical Reasoning Test	Verbal intellectual ability	
Psychomotor Vigilance Test - 3 Minute Version	Sustained attention	
Short Letter-N-Back Test - 2 Back Version	Working memory	
Short Visual Object Learning Test	Visual object learning	
Short Penn Continuous Performance Task	Visual attention	
Digit Symbol Test	Processing speed	
Penn Trailmaking Test B	Executive function	
Delayed Discounting Task	Reward decision-making	✓
Measured Emotion Differentiation Test	Emotion discrimination	✓
Penn Line Orientation Test	Spatial ability	✓
Penn Matrix Analysis Test	Abstraction & Mental flexibility	✓
Risk Discounting Task	Reward decision-making	✓

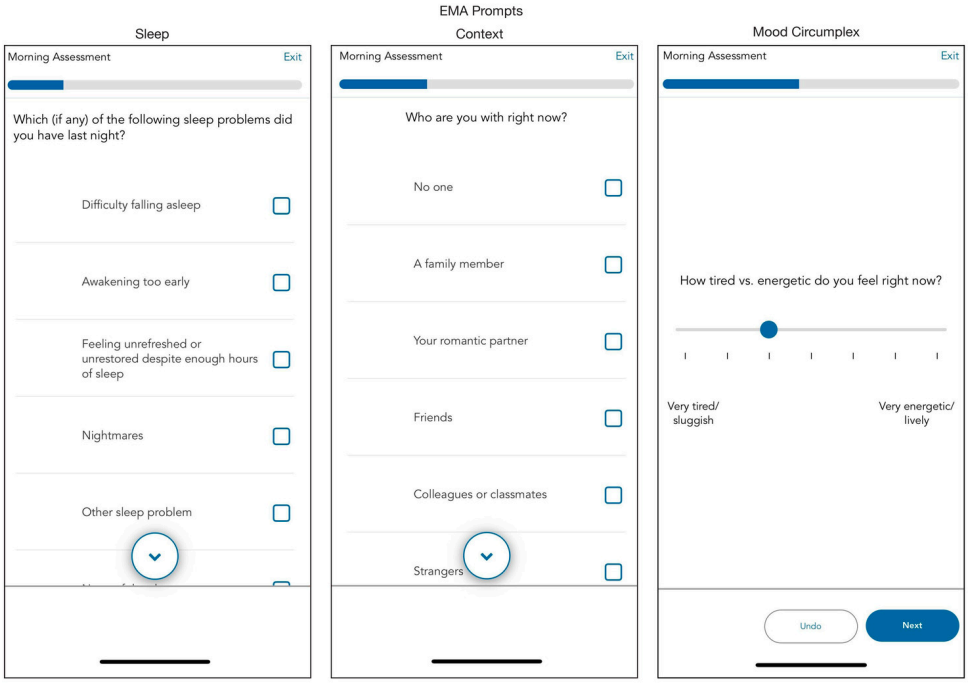

Figure 2. Curious EMA.

Examples of three EMA prompts featured within the daily morning activity are displayed.

and physical health. Descriptions of the specific items, procedures, and attribution are available through a Creative Commons License (Attribution-Non Commercial-Share Alike 4.0 International Creative Commons license agreement; CC BY-NC-SA 4.0). Versions of *REACH* are now being employed at several of the sites involved in an international collaborative effort on actigraphy and mood disorders (see below) that can enhance comparability and generalizability of the findings.

We configure the Curious app to send notification reminders prompting participants to complete the surveys at four daily time points: morning, mid-day, afternoon, and evening. Each participant determines the exact time when they receive these notification reminders based on their individual schedule. We assist participants in following general guidelines regarding when each assignment should be scheduled. For example, we advise participants that each assignment should be separated by at least two hours. The morning survey should open shortly after they wake up (typically assigned between 6:30-9AM). The evening survey should open shortly before participants go to bed (typically assigned between 10-11:30PM). The mid-day and afternoon surveys offer more flexibility but are usually assigned between 11AM and 5PM. Participants have a 60-minute window to complete each survey. The Curious app allows participants to skip or exit the survey if they choose. See Figure 2 for exemplar screenshots from Curious; the specific item prompts assigned across each of the four surveys are detailed in Supplementary Table 1.

ACTIGRAPHY

To measure physical activity and sleep,[86] participants wear the GENEActiv actigraphy device (GENEActiv, Activinsights Ltd, Kimbolton, UK). The GENEActiv is a waterproof wristwatch-like device that participants are instructed to wear continuously for three weeks after the imaging visit. The preexisting literature maintains that three weeks of actigraphy data is helpful to discern weekly variation in sleep and activity data.[87] The GENEActiv devices are configured to collect raw acceleration data at 66.7 Hz for 21 days.

As part of our initial data release, we provide raw binary files containing acceleration data along the three x, y, and z movement axes. Binary files are extracted with the GENEActiv software version 4.0.12. Raw accelerometer data are processed with the GGIR R package (version 3.2.0),[88] which performs auto-calibration, non-wear detection, and calculation of relevant sleep and physical activity variables. All processing is based on the Euclidean Norm Minus One (ENMO) metric with automated calibration. Acceleration angle metrics are calculated over 5-second epochs. Non-wear detection is performed using the 2023 algorithm, with an epoch length of 900 seconds for non-wear and signal clipping, and an epoch of 3600 seconds for non-wear detection. GGIR also evaluates the validity of each day and night of the study, requiring minimum valid wear time of 16 hours per day (midnight-midnight) and 12 hours per night (noon-noon). Sleep and wake are detected using the van Hees 2015 algorithm,[89,90] which identifies sustained inactivity periods as intervals of at least five minutes during which the arm angle variability remains lower than five degrees. The sleep period window is detected using the HDCZA guider algorithm,[89] which identifies the longest period

of low movement and posture change to find the main daily sleep period. The sleep period time (SPT) is then used to calculate sleep variables, including sleep duration, defined as the total time spent in sustained inactivity bouts within the SPT window; wake after sleep onset (WASO), defined as the total time spent awake between the start and end of SPT; and sleep efficiency, calculated as the ratio of sleep duration to the total length of the SPT. Daytime physical activity levels are defined using GGIR's default acceleration cutoff points of 40 mg for light, 100 mg for moderate, and 400 mg for vigorous activity. Sleep variables highlighted in the results section include total sleep duration (hours), WASO (hours), and sleep efficiency (%). Physical activity variables include time spent in light, moderate, and vigorous activity (in minutes). GGIR outputs several data quality variables, which we use to apply additional quality control. We first exclude recordings with device issues (e.g., clipping or failed calibration). Next, we exclude days or nights with poor data quality (e.g., >20% invalid data, >30% non-wear), as well as nights with abnormal features (extreme sleep durations < 2 or > 14 hours, extreme episode counts of < 5 or > 40, and daysleeper patterns). Finally, participants are excluded from each analysis if they have fewer than three valid days for activity analyses, and fewer than three valid nights for sleep analyses. Data from this study will be included in a collaborative effort with the Motor Activity Research Consortium for Health at the NIMH (mMARCH)[91]; that was established to harmonize the processing, data extraction, analytic methods and collection of common ancillary data for studies of mood disorders in adults and youth. In particular, mMARCH has made advances in processing accelerometry data[91] and statistical analytic methods.[92] Use of common procedures for actigraphy and EMA is now underway in several international settings (including the US, Brazil, Canada, Korea, and Switzerland) that will enhance the generalizability and interpretability of this research.

IMAGING ACQUISITION

MRI data is acquired on a 3T Siemens Magnetom Prisma (Erlangen, Germany) MRI scanner with the product 64-channel receiver array at the University of Pennsylvania. The in-person imaging session lasts one hour. The current study does not track motion during the scan. While we share all data collected, as in other work,[93] we recommend excluding fMRI runs with a median framewise displacement (FD) greater than 0.2 mm. Sequence parameters and file naming conventions are summarized in Table 4; a full protocol PDF and the EXAR file is also available (see Data Availability, below).

STRUCTURAL MRI

The imaging protocol begins with one run of T1-weighted (T1w) MPRAGE structural MRI (named **anat-T1w**) that is aligned with the ABCD study[94] (176 slices; repetition time, TR = 2500 ms; echo time, TE = 2.9 ms; flip angle, FA = 8°; field of view, FOV = 256x256 mm; matrix size = 256x256; voxel size = 1x1x1 mm; phase encoding direction = A >> P; acquisition time = 7:12). We also acquire the T2-weighted (T2w) SPACE structural image (named **anat-T2w**) used in the ABCD protocol (176 slices; TR = 3200 ms; TE = 565 ms; FA = 120°; FOV = 256x256 mm; matrix size = 256x256; voxel size = 1x1x1 mm; phase encoding direction = A >> P; acquisition time 6:35). Both scans use embedded volumetric navigators to perform real-time motion correction, reducing motion artifacts in the resulting anatomical images.[95]

FUNCTIONAL MRI

This study includes two runs of multi-echo EPI. Previous work has shown that multi-echo EPI scans facilitate the identification of person-specific variation in BOLD fMRI with far less data.[55] Before the fMRI time series are acquired, we collect PEpolar-style field maps for distortion correction of the fMRI data. These field maps (named **fmap-epi_acq-func_dir-AP** and **fmap-epi_acq-func_dir-PA**) consist of two multi-echo EPI acquisitions with the same acquisition parameters as the fMRI scans with opposite phase encoding directions (72 slices; TR = 13,690 ms; TE = 20.80, 58.48, 96.16, 133.84, 171.52 ms; FA = 90°; FOV = 220x220 mm; matrix size = 110x110; voxel size = 2x2x2 mm; acquisition time = 1:22). Current software cannot leverage multiple echoes in PEpolar-style field maps, so we retain the first echo from each multi-echo field map with `acq-func` (e.g., `sub-01_ses-01_acq-func_dir-AP_epi.nii.gz`). The multi-echo versions of the field maps are retained in the dataset for potential future use.

Two runs of functional MRI (named **func-bold_task-bao_dir-AP** and **func-bold_task-rat_dir-PA**) are acquired with a multiband EPI sequence (CMRR, University of Minnesota). Each functional run is acquired with the same protocol (72 slices; TR = 1761 ms; TE = 14.20, 38.93, 63.66, 88.39, 113.12 ms; FA = 68°; FOV = 220x220 mm; matrix size = 110x110; voxel size = 2x2x2 mm; multiband factor = 6; in-plane acceleration factor = 2). This protocol is highly similar to the one used by Moser et al. (2025)[96] and Siegel et al. (2024).[97] During each run, participants view Pixar short animated movies: "Bao" and "Your Friend the Rat." For "Bao," the phase encoding direction is anterior-to-posterior and each run is 7:13 minutes long, during which 246 volumes are acquired. For "Your Friend the Rat," the phase encoding direction is posterior-to-anterior and each run is 10:45 minutes long, during which 366 volumes are acquired. The current protocol builds upon literature showing that naturalistic movie stimuli is more reliable in measuring functional connectivity than resting-state measures[98] and better at predicting individual differences.[99] Furthermore, studies that synchronize film-viewing across participants support analyses like functional alignment and inter-subject functional correlation.[100] Film-viewing stimuli also permits manual or automated annotation used in performing task-related analyses.[101-103] Finally, studies have shown that film-viewing reduces head motion in the scanner among children[104] and past developmental studies have also relied upon movie stimuli.[105,106] For both runs, a single-band reference image is also acquired for each echo to assist with co-registration. Furthermore, three no-excitation noise volumes are also acquired at the end of

Table 4. Imaging Parameters.

Sequence	Slices	% FOV Phase	Resolution (mm)	TR (ms)	TE (ms)	TI (ms)	Flip Angle (°)	Multi Band Accel	Phase Partial Fourier
anat-T1w	176	100%	1.0x1.0x 1.0	2500	2.9	1070	8	N/A	Off
anat-T2w	176	100%	1.0x1.0x 1.0	3200	565	N/A	120	N/A	Allowed
fmap-epi_acq-func_dir-AP	72	100%	2.0x2.0x 2.0	13690	20.80, 58.48, 96.16, 133.84, 171.52	N/A	90	N/A	6/8
fmap-epi_acq-func_dir-PA	72	100%	2.0x2.0x 2.0	13693	20.80, 58.48, 96.16, 133.84, 171.52	N/A	90	N/A	6/8
func-bold_task-bao_dir-AP	72	100%	2.0x2.0x 2.0	1761	14.20, 38.93, 63.66, 88.39, 113.12	N/A	68	6	6/8
func-bold_task-rat_dir-PA	72	100%	2.0x2.0x 2.0	1761	14.20, 38.93, 63.66, 88.39, 113.12	N/A	68	6	6/8
dwi-dwi_acq-HASC92_dir-AP	84	100%	1.7x1.7x 1.7	4300	90	N/A	90	4	7/8
fmap-epi_acq-dwi_dir-PA	84	100%	1.7x1.7x 1.7	4300	90	N/A	90	4	7/8
perf-asl	44	100%	3.0x3.0x 3.0	5000	10.8	N/A	120	N/A	N/A
anat-MEGRE_acq-1p5mm	96	75%	1.5x1.5x 1.5	35	7.5, 15, 22.5, 30	N/A	15	N/A	Off

each run to allow for implementation of denoising with NORDIC.[96,107,108] Finally, we acquire all fMRI data with both magnitude and phase reconstruction enabled; this complex data is helpful for denoising with NORDIC, improves T2* estimation, and allows for cutting edge distortion correction methods (e.g., MEDIC).[109]

DIFFUSION MRI

This study includes compressed-sensing diffusion spectrum imaging (CS-DSI). The vast majority of dMRI images sample many directions at one or more *b*-values (or shells). In contrast, DSI scans densely sample *q*-space on a Cartesian grid. This enables the direct estimation of the diffusion Ensemble Average Propagator (EAP), the physical process driving biologically meaningful derivatives of dMRI.[110] Previous research has demonstrated that DSI achieves greater biological fidelity in tractography when compared to ground-truth anatomic tracings through more accurate ODF estimates.[111,112] DSI scans have also been shown to result in improved tractography[113] and enhanced gray-white contrast.[114] While available research emphasizes massive potential for DSI, the dense Cartesian sampling requires very long scan times (30+ minutes), which has prohibited the wide use of DSI.

To mitigate the need for long DSI scan times, recent work has shown that CS-DSI acquisitions can undersample *q*-space and still accurately estimate the underlying EAPs.[115-120] Our team recently published the first in-depth study that compared CS-DSI and full DSI scans in humans.[57] We found that a 7.4-minute CS-DSI scan provided highly similar accuracy and reliability to a full DSI scan. This study acquires a 92-direction CS-DSI scan (named **dwi-dwi_acq-HASC92_dir-AP**) that uses a homogenous angular sampling scheme (HA-SC[121]; TR = 4300 ms; TE = 90.00 ms; FOV = 230x230 mm; voxel size = 1.7x1.7x1.7 mm; 84 interleaved slices acquired anterior to posterior; a multiband factor of 4; acquisition time = 9:02).[118] In addition to 95 diffusion-weighted images, 9 *b* = 0 images are acquired (104 volumes total). For full details on the CS-DSI sampling schemes see Data Availability, below. dMRI data is acquired with both magnitude and phase reconstruction enabled; this complex data is helpful for denoising with Marchenko-Pastur principal components analysis (MP-PCA; as described below). For distortion correction, we acquire a reverse phase-encoded scan (named **fmap-epi_acq-dwi_dir-PA**) that includes 7 volumes (TR = 4300 ms; TE = 90.00 ms; FOV = 230x230 mm; voxel size = 1.7x1.7x1.7 mm; 84 interleaved slices acquired posterior to anterior; multiband factor = 4; acquisition time = 2:09).

ARTERIAL SPIN-LABELED MRI

To measure brain perfusion, we acquire a state-of-the-art arterial spin-labeled (ASL) MRI scan. Specifically, we use a background-suppressed unbalanced PCASL scan (named **perf-asl**) using a stack of spirals turbo spin echo (Labeling duration = 1.8 s, Post-labeling delay [PLD] = 1.8 s, TR = 5000.0 ms; TE = 10.8 ms; FOV = 240x240 mm; voxel size = 3.0x3.0x3.0 mm; acquisition time = 4:24).[122,123] We also acquire a reference scan to assist in ASL calibration (M0 and T1 estimation) and co-registration, using the same sequence to acquire a presaturated, unsuppressed proton-density weighted volume (Tsat = 5 s) and presaturated inversion recovery volume (Tsat = 5 s, TI = 1.978 s). This reference scan can be used to calculate a low-resolution quantitative T1 map.[124]

MEGRE

We acquire one run of multi-echo gradient-recalled echo (MEGRE; named **anat-MEGRE_acq-1p5mm**) scan with magnitude and phase reconstruction (96 slices; repetition time, TR = 35 ms; echo times, TEs = 7.5, 15, 22.5, 30 ms; flip angle, FA = 15°; field of view, FOV = 180x240 mm; matrix size = 120x160; voxel size = 1.5x1.5x1.5 mm; phase encoding direction=A >> P; acquisition time = 3:59). This scan can be used for quantitative susceptibility mapping (QSM), which is sensitive to developmental changes in brain iron and myelin.

IMAGE PROCESSING

As part of our initial data release, we provide processed T1w, fMRI, dMRI, and ASL images. sMRIPrep is used for processing T1w and T2w images. fMRIPrep is used to minimally preprocess fMRI data[125]; fMRI post-processing is performed with fMRIPost-AROMA,[126] tedana,[127] and XCP-D.[128] dMRI is processed with QSIPrep and QSIRecon.[129] ASL images are processed with ASLPrep.[130] As of the current data release, we do not provide processed MEGRE/QSM images.

STRUCTURAL IMAGE PROCESSING

Preprocessing of T1-w images uses sMRIPrep 0.16.0, as implemented in fMRIPrep 24.1.1[125] using Nipype 1.8.6.[131, 132] The T1w image undergoes correction for intensity non-uniformity with N4BiasFieldCorrection with ANTs 2.5.3,[133, 134] skull-stripping with a Nipype implementation of the ANTs brain extraction workflow, and brain tissue segmentation with FSL's FAST 6.0.7.7.[135] Brain surfaces are reconstructed using FreeSurfer 7.3.2,[136] and the brain mask estimated previously is refined with a custom variation of the method to reconcile ANTs-derived and FreeSurfer-derived segmentations.[137] The T2w image is used to improve pial surface refinement. Volume-based spatial normalization to two standard spaces (MNI152NLin6Asym and MNI152NLin2009cAsym, accessed through TemplateFlow 24.2.0)[138] is performed through nonlinear registration with antsRegistration (ANTs 2.5.3), using brain-extracted versions of both T1w reference and the T1w template. A CIFTI grayordinate file containing 91k vertices is resampled onto the fsLR template using Connectome Workbench.[139,140]

FUNCTIONAL IMAGE PREPROCESSING

fMRI data is preprocessed using fMRIPrep 24.1.1,[125,141] which is based on Nipype 1.8.6.[131,132] First, a B_0-nonuniformity map is estimated based on echo-planar imaging (EPI) references using FSL's TOPUP.[142] For each BOLD run, the following preprocessing is performed. First, a reference volume is generated from the shortest echo of the BOLD run for use in head-motion correction. Head-motion parameters with respect to the BOLD reference (transformation matrices, and six corresponding rotation and translation parameters) are estimated before any spatiotemporal filtering using FSL's mcflirt.[143] The estimated field map is aligned with rigid-registration to the target EPI reference run. The BOLD reference is then co-registered to the T1w reference using FreeSurfer's bbregister[144] with six degrees of freedom. The aligned T2w image is also used for initial co-registration. The BOLD time series are resampled onto the left/right-symmetric template "fsLR" using Connectome Workbench.[139,140] A "goodvoxels" mask is applied during volume-to-surface sampling in fsLR space, excluding voxels whose time series have a locally high coefficient of variation. Grayordinates files[139] containing 91k samples are also generated with surface data transformed directly to fsLR space and subcortical data transformed to 2 mm resolution MNI152NLin6Asym space.

POST-PROCESSING OF FUNCTIONAL IMAGES

Following preprocessing with fMRIPrep, images are post-processed with complementary software. We seek to decompose the processed fMRI time series into "noise" and "signal" components using two methods. First, ICA-AROMA[126,145] is implemented using fMRIPost-AROMA 0.0.10, which is based on Nipype 1.9.2.[131,132] Noise and signal components from ICA-AROMA are compared to tedana,[146] which is run using the "minimal" decision tree – a simplified version of the MEICA decision tree. Tedana fits a monoexponential model to the data at each voxel using nonlinear model fitting to estimate T2* and S0 maps, using T2*/S0 estimates from a log-linear fit as initial values. For each voxel, the value from the adaptive mask is used to determine which echoes would be used to estimate T2* and S0. In cases of model fit failure, T2*/S0 estimates from the log-linear fit are retained instead. Multi-echo data are then optimally combined using the T2* combination method.[147] Next, component selection is performed to identify BOLD (TE-dependent) and non-BOLD (TE-independent) components using a decision tree. Rejected components' time series are then orthogonalized with respect to accepted components' time series. Minimum image regression is then applied to the data to remove spatially diffuse noise.[146] The tedana workflow uses NumPy,[148] SciPy,[149] pandas,[150] scikit-learn,[151] Nilearn,[152] Bokeh,[153] Matplotlib,[154] and Nibabel.[155]

After tedana is applied, the component classifications from fMRIPost-AROMA and tedana are combined, such that any component that is rejected by either ICA-AROMA or

ME-ICA is labeled as rejected. The rejected components' time series are then orthogonalized with respect to accepted components' time series. Minimum image regression is then applied to the mixing matrix in order to remove spatially diffuse noise.[146]

Following identification of noise components using ICA-AROMA and tedana, images are processed using XCP–D.[128, 156,157] XCP-D is built with Nipype 1.9.2.[131,132] Many internal operations of XCP-D use AFNI,[158,159] Connectome Workbench,[139,140] ANTS,[160] TemplateFlow 24.2.2,[138] Matplotlib 3.10.0,[154] Nibabel 5.3.2,[155] Nilearn 0.11,[152] NumPy 2.2.1,[161] pybids 0.18.1,[162] and SciPy 1.15.1.[149]

Non-steady-state volumes are extracted from the preprocessed confounds and are discarded from both the BOLD data and nuisance regressors. The set of orthogonalized nuisance components from the tedana step is selected for the nuisance regression, along with mean white matter signal, mean cerebrospinal fluid signal, and mean global signal.[157,163] The BOLD data are converted to NIfTI format, despiked with AFNI's 3dDespike, and converted back to CIFTI format. Nuisance regressors are regressed from the BOLD data using a denoising method based on Nilearn's approach. The time series are band-pass filtered using a second-order Butterworth filter, in order to retain signals between 0.01-0.08 Hz. The same filter is applied to the confounds. The resulting time series are then denoised using linear regression. The denoised BOLD is then smoothed using Connectome Workbench with a Gaussian kernel (FWHM = 6 mm).

Processed functional time series are extracted from residual BOLD using Connectome Workbench[139,140] for the atlases. Corresponding pairwise functional connectivity between all regions is computed for each atlas, which is operationalized as the Pearson's correlation of each parcel's unsmoothed time series with the Connectome Workbench. In cases of partial coverage, uncovered vertices (values of all zeros or NaNs) are either ignored (when the parcel had >50.0% coverage) or the whole parcel is set to zero (when the parcel had <50.0% coverage). The following atlases are used in the workflow: the Schaefer Supplemented with Subcortical Structures (4S) atlas[139,164-167] at 10 different resolutions (156, 256, 356, 456, 556, 656, 756, 856, 956, and 1056 parcels), the Glasser atlas,[168] the Gordon atlas,[169] the Tian subcortical atlas,[170] the HCP CIFTI subcortical atlas,[139] and the MIDB precision brain atlas derived from ABCD data and thresholded at 75% probability.[171] In addition, XCP-D calculates two scalar maps. First, the amplitude of low-frequency fluctuation (ALFF)[172] is computed by transforming the mean-centered, standard deviation-normalized, denoised BOLD time series to the frequency domain. The power spectrum is computed within the 0.01-0.08 Hz frequency band and the mean square root of the power spectrum is calculated at each voxel to yield voxel-wise ALFF measures. The resulting ALFF values are then multiplied by the standard deviation of the denoised BOLD time series to retain the original scaling. The ALFF maps are smoothed with the Connectome Workbench using a Gaussian kernel (FWHM = 6 mm). Second, for each hemisphere, regional homogeneity (ReHo)[173] is computed using surface-based 2dReHo.[174] Specifically, for each vertex on the surface, Kendall's coefficient of concordance (KCC) is computed with nearest-neighbor vertices to yield ReHo. For the subcortical, volumetric data, ReHo is computed with neighborhood voxels using AFNI's 3dReHo.[175]

DMRI PROCESSING

dMRI preprocessing is performed using QSIPrep 1.0.0,[129] which is based on Nipype 1.9.1[131,132]; (RRID:SCR_002502). Many internal operations of QSIPrep use Nilearn 0.10.1[152] (RRID:SCR_001362) and Dipy.[176] QSIPrep uses a slightly different anatomical workflow than sMRIPrep/fMRIPrep. Specifically, the T1w image is corrected for intensity non-uniformity (INU) and used as the T1w-reference map. The anatomical reference image is first reoriented into AC-PC alignment using the 6-degrees-of-freedom (rigid) component of a full affine registration to MNI152NLin2009cAsym, and a symmetric nonlinear registration (SyN) using antsRegistration to further refine alignment to the MNI152NLin2009cAsym template. Brain extraction is performed on the T1w image using SynthStrip[177] and automated segmentation is performed using SynthSeg[178] from FreeSurfer version 7.3.1.

Next, any diffusion images with a b-value less than 100 s/mm^2 are treated as a b = 0 image. Magnitude and phase diffusion-weighted imaging data are combined into a complex-valued file, then denoised using the Marchenko-Pastur PCA method implemented in MRtrix3's dwidenoise[179-181] with a 3-voxel window. After denoising, the complex-valued data are split back into magnitude and phase. The mean intensity of the diffusion-weighted series is adjusted so all the mean intensity of the b = 0 images matched across each separate DWI scanning sequence.

Initial motion correction is performed using only the b = 0 images. An unbiased b = 0 template is constructed over two iterations of 3dSHORE registrations. To estimate head motion in b>0 images, the SHORELine method[57,129] is used to iteratively leave out each b>0 image and reconstruct the remaining images using 3dSHORE[116]; the signal for the left-out image served as the registration target. The reconstructed, model-generated images are transformed into alignment with each b>0 image. Both slicewise and whole-brain quality control measures (cross correlation and R^2) are calculated.

Susceptibility distortion correction is performed using DRBUDDI,[182] part of the TORTOISE[183] software package. Reverse phase-encoding EPI-based field maps are collected, resulting in pairs of images with distortions going in opposite directions. DRBUDDI uses b = 0 reference images with reversed phase encoding directions to estimate the susceptibility-induced off-resonance field. A T2-weighted image is included in the multimodal registration. The DWI time series are resampled to AC-PC, generating a preprocessed DWI run in AC-PC space with 1.7 mm isotropic voxels.

Following preprocessing, the preprocessed dMRI images are reconstructed using QSIRecon (1.0.1).[129] Diffusion orientation distribution functions (ODFs) are reconstructed using generalized q-sampling imaging (GQI)[184] with a ratio of mean diffusion distance of 1.250000 in DSI Studio (ver-

sion 94b9c79). Automatic Tractography is run in DSI Studio (version 94b9c79) and bundle shape statistics are calculated.[185]

ASL IMAGE PROCESSING

Arterial spin-labeled MRI images are preprocessed using ASLPrep 0.7.5,[130,186] which is based on fMRIPrep[125,187] and Nipype 1.8.6.[131] Many internal operations of ASLPrep use Nilearn 0.11.1,[152] NumPy,[161] and SciPy.[149] In large part, ASLPrep uses the precomputed structural image processing from sMRIPrep, as described above. The ASL reference scan is co-registered to the T1w reference using Freesurfer's bbregister which implements boundary-based registration[144] with six degrees of freedom. All resampling in ASLPrep uses a single interpolation step that concatenates all transformations. Gridded (volumetric) resampling is performed using antsApplyTransforms, configured with Lanczos interpolation to minimize the smoothing effects of other kernels.[188]

Head-motion parameters are estimated for the ASL data using FSL's mcflirt.[143] Motion correction is performed separately for label and control volumes in order to account for intensity differences between different contrasts; when these volumes are motion corrected together, intensity differences can be conflated with head motions.[189] Next, ASLPrep concatenates the motion parameters across volume types and re-calculates relative root mean-squared deviation. Several confounding time series are calculated, including both framewise displacement (FD) and DVARS. FD and DVARS are calculated using the implementations in Nipype (following the definition by Power et al., 2014[190]) for each ASL run. ASLPrep summarizes in-scanner motion as the mean framewise displacement and relative root-mean square displacement.

ASLPrep is used to calculate cerebral blood flow (CBF) from the single-delay PCASL using a single-compartment general kinetic model.[191] Calibration (M0) volumes associated with the ASL scan are smoothed with a Gaussian kernel (FWHM = 5 mm) and the average calibration image is calculated and scaled by 10.0. The quality evaluation index (QEI) is computed for each CBF map.[192] QEI is based on the similarity between the CBF and the structural images, the spatial variability of the CBF image, and the percentage of gray matter voxels containing negative CBF values.

Parcellated CBF estimates are extracted for multiple atlases, including the Schaefer Supplemented with Subcortical Structures (4S) atlas[139,164-167] at 10 different resolutions (156, 256, 356, 456, 556, 656, 756, 856, 956, and 1056 parcels), the Glasser atlas,[168] the Gordon atlas,[169] the Tian subcortical atlas,[170] and the HCP CIFTI subcortical atlas.[139] In cases of partial coverage, either uncovered voxels (values of all zeros or NaNs) are ignored (when the parcel has >50.0% coverage) or the whole parcel is set to zero (when the parcel has <50.0% coverage).

RESULTS

Here we present initial data from the first participants enrolled in the study protocol. As described below, we focus on EMA, actigraphy, and neuroimaging data. Notably, all processed data described below are openly available on OpenNeuro; all processing code and software is available on GitHub (see Data and Code Availability, below). Data will be updated regularly as study accrual continues.

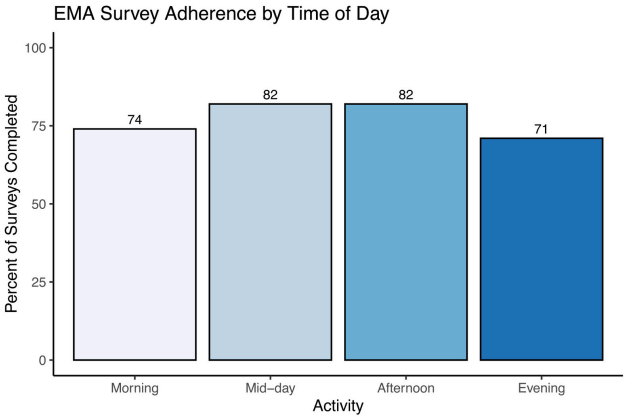

Figure 3. EMA adherence.

Average adherence for each survey across the 14-day EMA period is displayed for each of the four daily timepoints.

ECOLOGICAL MOMENTARY ASSESSMENT

A total of n = 7 completed the 14-day EMA procedure in this preliminary data release; EMA was not available for the first three study participants enrolled. We examined participant compliance with the EMA procedure according to time of day over the study period by calculating the percentage of prompts to which participants responded for each time point (Figure 3). The current study's EMA adherence averaged 72% across all activities, with compliance of 74% in the morning, 82% at mid-day, 82% in the afternoon, and 71% in the evening. In addition to adherence, we examined mean scores and daily patterns in mood circumplex items (Figures 4 & 5). Out of a 7-point scale, we found a mean sadness score of 3.50 (SD = 0.91), a mean anxiousness score of 3.67 (SD = 0.96), a mean positive thoughts score of 4.30 (SD = 1), a mean negative thoughts score of 3.49 (SD = 0.86), a mean active score of 3.20 (SD = 1.16), and a mean tiredness score of 3.46 (SD = 1.18).

ACTIGRAPHY

A sample of n = 6 participants completed the 21-day actigraphy procedure; actigraphy devices were not available for the first four participants enrolled in the study. We examined participants' 24-hour sleep timing patterns through two measures: sleep onset and wake up (Figure 6). The preliminary data revealed differences in monophasic (i.e., single peak in the density plot of sleep onset) and biphasic (i.e., two peaks in the density plot of sleep onset) sleep patterns between participants. The occurrence of multiple peaks in a participant's density plot suggests irregularity in sleep onset and wake up times. In addition to 24-hour sleep timing patterns, we explored daily sleep and physical activity patterns over multiple days and nights (Figure 7). Daily

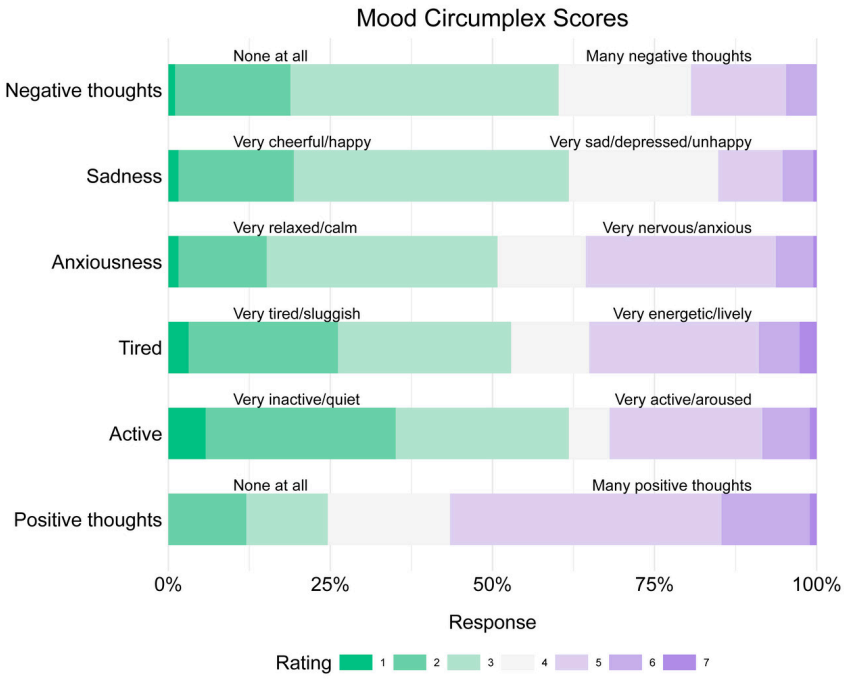

Figure 4. Ecological momentary assessment (EMA) mood scores.

The proportion of mood circumplex scores across participants and timepoints are displayed. Each mood score is represented by a horizontal bar, with colors indicating rating intensity on a 1-7 scale. The length of each colored segment shows the proportion of responses at each rating level across participants and activity types (morning, mid-day, afternoon, and evening assessments). Green represents lower ratings (1-2), light gray represents neutral ratings (3-5), and purple represents higher ratings (6-7). The specific meaning of high and low ratings varies for each measure as indicated by the labels on either side of the bars. For example, in 'Sadness,' a longer green segment indicates more responses of 'Very cheerful/happy' while a longer purple segment indicates more responses of 'Very sad/depressed/unhappy.'

sleep metrics included sleep duration, wake after sleep onset (WASO; time spent awake after sleep onset but before the official wake up time), and sleep efficiency (the percentage of time asleep while in bed). The data collected for the 21-day actigraphy period revealed a mean sleep duration of 6.78 hours (SD = 1.22), a mean wake after sleep onset period of 1.34 hours (SD = 0.73), and mean sleep efficiency of 82% across participants (SD = 6.68). The data also highlighted distinct levels of physical activity (e.g., light activity, moderate activity, and vigorous activity). Light activity refers to an acceleration greater than 40 milli-g (mg), moderate activity refers to an acceleration greater than 100 mg, and vigorous activity refers to an acceleration greater than 400 mg. The actigraphy data revealed an across subject average of mean light activity level of 150 minutes per day (SD = 41.6), a mean moderate activity level of 130 minutes per day (SD = 43.7), and a mean vigorous activity level of 4.79 minutes per day (SD = 6.31).

NEUROIMAGING

Neuroimaging data was collected on all n = 10 participants. Preprocessed structural MRI data exhibited expected mean cortical thickness, curvature, and sulcal depth across the sample (Figure 8). In addition, cerebral blood flow estimates from the ASL images displayed expected patterns of perfusion, with greater cerebral blood flow in cortical gray matter than white matter (Figure 9). For the multi-echo fMRI data, as expected, T2* did not change dramatically by including or excluding NORDIC denoising (Supplementary Figure 1). Notably, tedana and AROMA showed relatively high levels of agreement on the classification of noise components (Supplementary Figure 2A). However, tedana appeared to be more sensitive, identifying some noise components that AROMA did not. In contrast, AROMA classified very few components as noise that tedana did not identify. The noise components only identified by tedana explained somewhat lower variance than the components that both methods identified as noise (Supplementary Figure 2B). All of the first 10 participants scanned had acceptable in-scanner motion (Supplementary Figure 3). Mean correlation matrices for the "Bao" and "Your Friend the Rat" video watching tasks derived from fully processed fMRI data revealed expected patterns of functional connectivity across all runs (Figure 10). This includes higher levels of within network connectivity and lower observed between network connectivity. Finally, diffusion imaging data collected using CS-DSI displayed expected patterns of generalized fractional anisotropy (GFA) and mean diffusivity (MD), with GFA being higher in white matter and MD being higher in gray matter (Figure 11). Reconstructed white matter bundles in three exemplar participants revealed excellent delineation of individual-specific white matter tracts (Figure 11C).

DISCUSSION

This study aims to provide high-quality brain and behavioral data to investigate affective dynamics in youth. Specifically, measures include advanced multimodal imag-

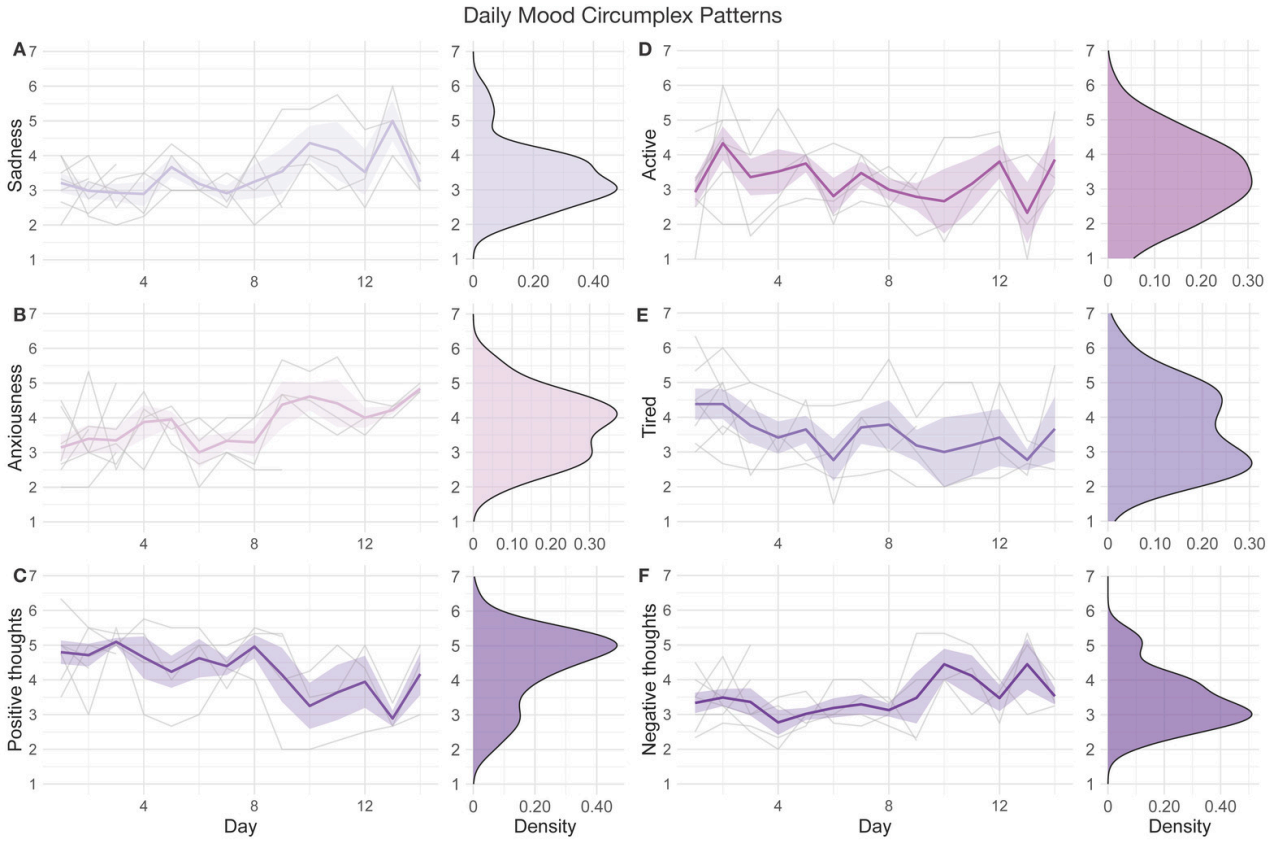

Figure 5. Ecological momentary assessment (EMA) daily mood patterns.

Daily patterns for each participant across the 14-day EMA period are shown for mood circumplex items: (**A**) sadness, (**B**) anxiousness, (**C**) positive thoughts, (**D**) active, (**E**) tired, and (**F**) negative thoughts. For each mood circumplex item, the left-side figure displays the score of 1 through 7 for each of the 14 days, with individual trajectories (gray lines), the mean group trajectory (colored line), and standard errors (colored shade). The right-side figure displays the distribution density of each score for that mood circumplex item across all days and participants.

ing, EMA, retrospective self-report questionnaires, computerized cognitive assessments, and actigraphy measures. Below we briefly discuss relevant context, limitations, and important future directions.

Difficulties in affective regulation during childhood may confer increased risk for psychopathology in adulthood. Children rely on social interactions to regulate their mood by seeking reassurance from others, eventually developing an internal self-regulation mechanism to manage their affective state.[1] Deficits in the child-caregiver relationship and early exposure to trauma may contribute to the development of affective instability.[1,193] Affective instability involves acute fluctuations in affect and is linked to aberrant development of psychological and psychosocial capabilities (i.e., shortfalls in self-esteem, social interactions, and sense of identity) and increased vulnerability to psychopathology later on.[1,194]

While affective instability is present in multiple psychiatric disorders, it has typically been studied within a single diagnosis using a case-control design, limiting the ability to examine common brain circuits impacted across diagnoses.[195,196] Affective instability is not only a diagnostic criterion of borderline personality disorder (BPD)[197] but is also observed in diverse conditions seen among adolescents and young adults, including bipolar disorder,[2] major depressive disorder (MDD)[2] and attention-deficit hyperactivity disorder (ADHD).[2] Existing evidence suggests that affective instability is associated with suicide threats and attempts among participants with BPD[4] as well as suicidal ideation in adults with other psychiatric disorders (e.g., depression, anxiety).[198] To extend prior work studying affective instability beyond traditional diagnostic categories, this study characterizes affective instability through a transdiagnostic, dimensional approach. Dimensional approaches to studying psychopathology have the potential to enhance the understanding of how maladaptive behaviors gradually evolve across development.[196] By recruiting a community sample of youth and collecting moment-to-moment information on affective dynamics, passive physical activity and sleep data, and high-quality neuroimaging data, the data from this study may accelerate research linking brain circuits to affective instability as a transdiagnostic construct.

In addition to densely sampled behavioral and clinical measures, this study leverages cutting-edge neuroimaging methods – such as multi-echo fMRI – to examine the neural substrates of affective dynamics. As a result of small effect sizes, previous neuroimaging work on mental illness has often required very large sample sizes to reliably identify relationships between brain features and behavioral

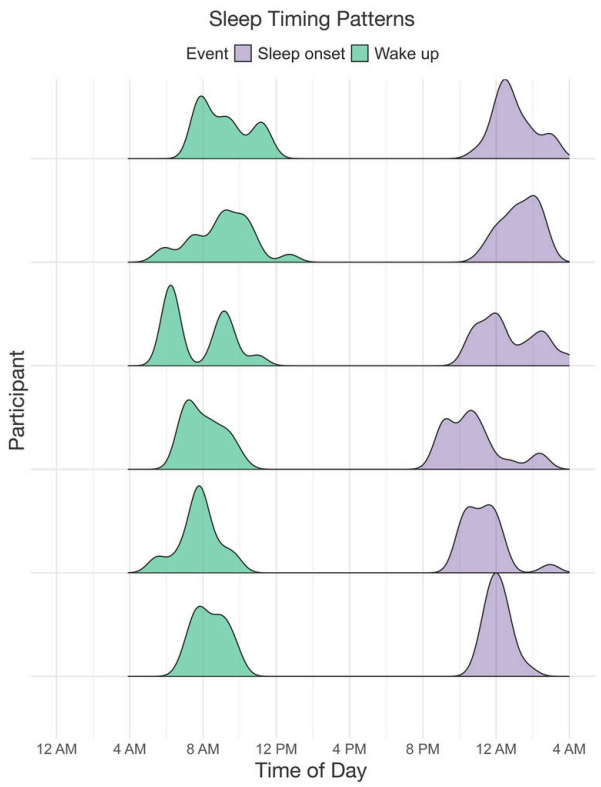

Figure 6. Sleep onset and wake timing.

Distributions of sleep onset and wake times over a 24-hour period are displayed, with purple indicating sleep onset and green indicating wake up for each participant who completed the actigraphy procedure.

phenotypes.[46,48,199,200] However, by adopting measures to enhance reliability and detection of individual-specific variation, studies may potentially mitigate the need to rely on large samples to identify meaningful brain-behavior associations.[51] One promising approach that could be used with this data is the personalized mapping of individuals' functional neuroanatomy, which has been shown to better predict behavioral phenotypes than group average parcellations.[201,202] Personalized functional networks (PFNs) account for individual variation in brain organization and have the potential to enhance the sensitivity of fMRI data to diagnosis-specific variation.[202,203] For example, expanded topography of the frontostriatal salience network defined using PFNs has been shown in individuals with depression.[204] In developmental cohorts, PFN topography is refined through childhood and adolescence and exhibits prominent sex differences.[205,206] These findings highlight the potential for studying PFNs in a youth population.

Although the current study introduces important advances, several limitations should be acknowledged. The study aims to capture the developmental relevance of affective instability through a community sample of 13- to 23-year-old participants. However, participants are only measured at one time point, precluding inference on within-individual development. Furthermore, because the current participant pool is collected through community sampling, and participants do not complete a diagnostic interview, the study does not examine specific clinical diagnoses. Despite the study's use of multi-echo fMRI, the current dataset does not collect very long timeseries or repeated sessions of fMRI data like some precision neuroimaging studies.[203,207,208] Furthermore, it should be noted that the projected sample size of N = 100 is unlikely to be adequately powered for studies of individual differences for most phenotypes, including those related to affective instability,[46,209] despite advances in behavioral assessment (e.g., EMA) and neuroimaging methods (e.g., multi-echo fMRI).

Taken together, this study provides a novel data resource to examine affective dynamics using brain and behavioral approaches – including EMA sampling, actigraphy data collection, and multi-echo fMRI. Moving forward, future longitudinal studies of brain development that examine participants pre- and post-adolescence may more fully characterize the developmental progression of affective instability, especially in clinical populations. We hope that this data resource will contribute to the identification of early markers of affective instability and emotion dysregulation before they develop into more severe psychopathology.

DATA AND CODE AVAILABILITY

All raw and processed imaging data is available on OpenNeuro: Raw https://openneuro.org/datasets/ds006131; MRIQC https://openneuro.org/datasets/ds006143; QSIPrep https://openneuro.org/datasets/ds006182; QSIRecon https://openneuro.org/datasets/ds006184; fMRIPrep https://openneuro.org/datasets/ds006185; ASLPrep https://openneuro.org/datasets/ds006188; fMRIPost-AROMA https://openneuro.org/datasets/ds006189; tedana https://openneuro.org/datasets/ds006190; tedana & AROMA https://openneuro.org/datasets/ds006191; XCP-D https://openneuro.org/datasets/ds006192. All analysis code for this project is openly available on GitHub: https://github.com/PennLINC/affective-instability.

ACKNOWLEDGMENTS

This study was supported by the AE Foundation, The Dean's Innovation Fund at the University of Pennsylvania Perelman School of Medicine, and the Penn/CHOP Lifespan Brain Institute. Additional support was provided by grants from the National Institute of Health: R01MH113550 (T.D.S.), R01MH112847 (R.T.S.), R01EB022573 (T.D.S.), R37MH125829 (T.D.S & D.A.F.), R01MH117014 and R01MH119219 (R.C.G., R.E.G.), K23 MH133118 (E.B.B.), BBRF #31319 (E.B.B.), R01EB031080 (J.A.D., M.D.T, & M.T.), BBRF #30837 (S.S.), BWF 1022955 CAMS (S.S.), DP5OD036142 (S.S.), U24NS130411 (D.W.), S10OD023495 (D.W.), F31MH136685 (J.B.).

CONFLICTS OF INTEREST

MT is employed by Siemens Medical Solutions USA

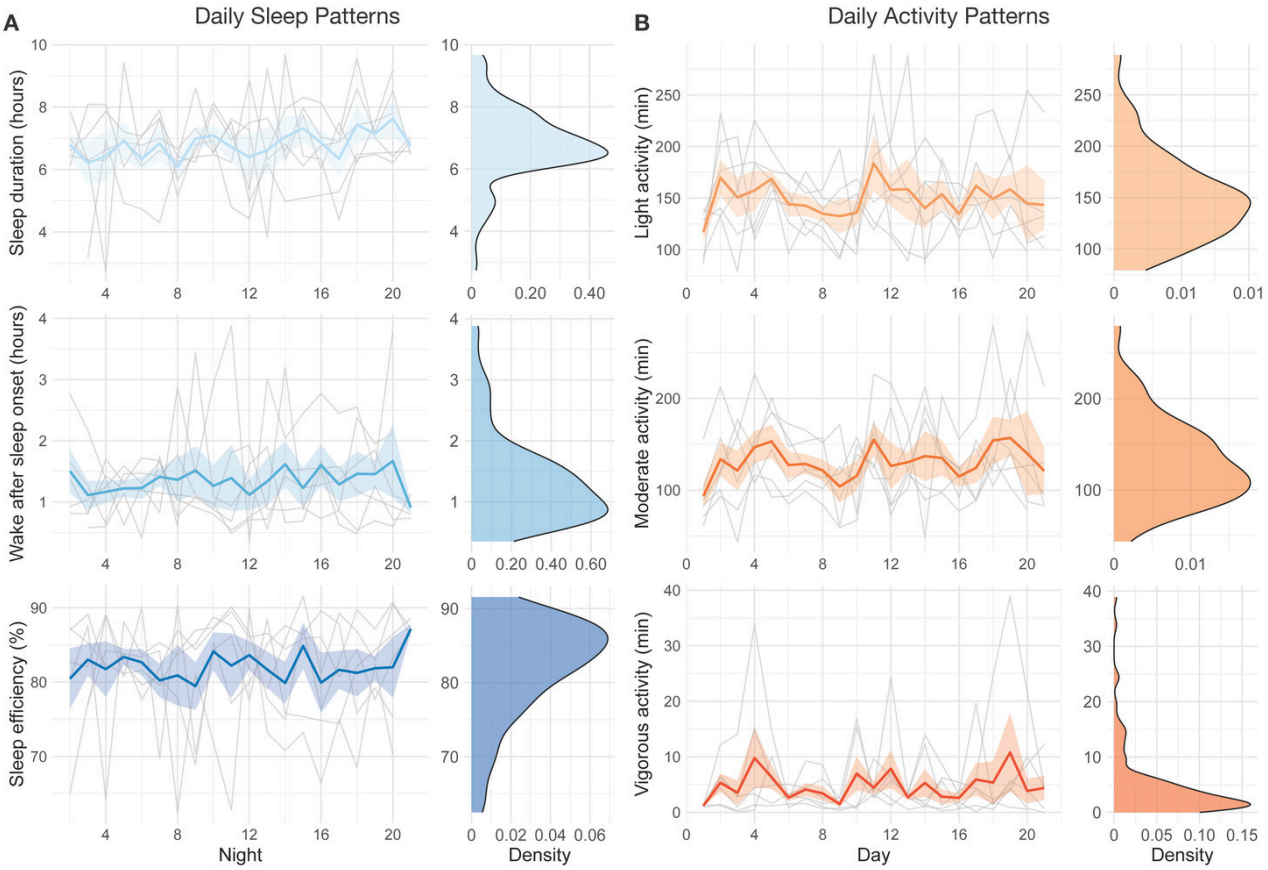

Figure 7. Daily sleep and physical activity patterns.

Daily patterns for each participant across the 21-day actigraphy period are shown for: (**A**) daily sleep patterns (sleep duration, wake after sleep onset, and sleep efficiency) and (**B**) daily activity patterns (light activity, moderate activity, and vigorous activity). For each actigraphy measure, the left-side figure displays the measure across the 21 days, with individual trajectories (gray lines), the mean group trajectory (colored line), and standard errors (colored shade). The right-side figure displays the distribution density of the actigraphy measure.

Submitted: April 30, 2025 CDT. Accepted: November 20, 2025 CDT. Published: January 26, 2026 CDT.

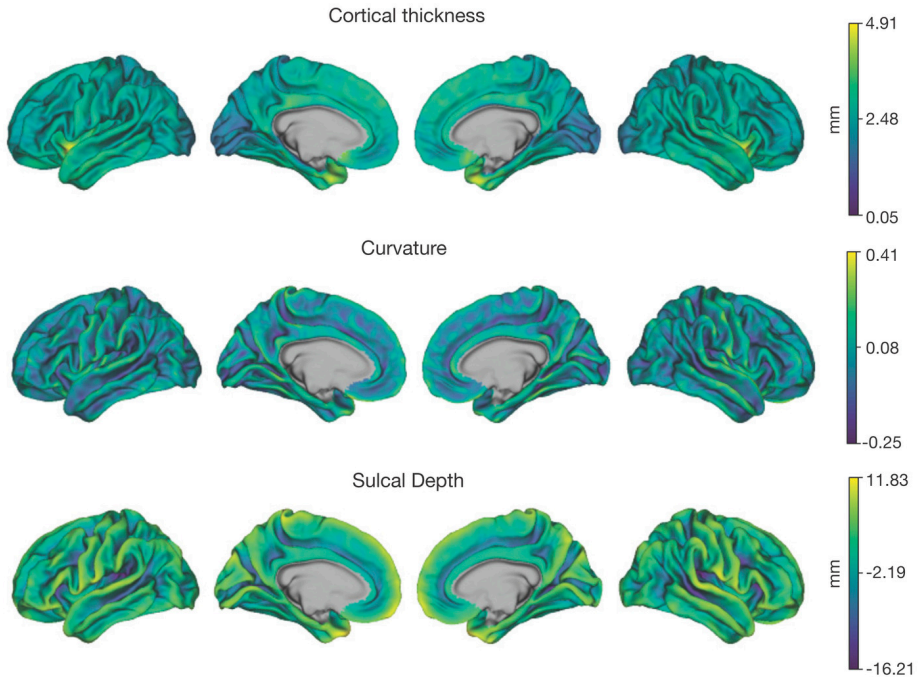

Figure 8. Anatomical MRI.

Mean cortical thickness, curvature, and sulcal depth across the initial sample are displayed.

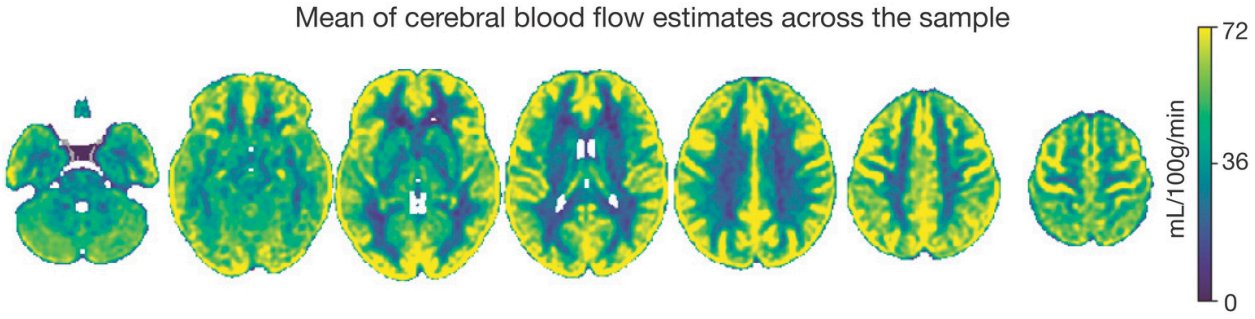

Figure 9. ASL cerebral blood flow.

The mean of cerebral blood flow estimates across the initial sample is displayed.

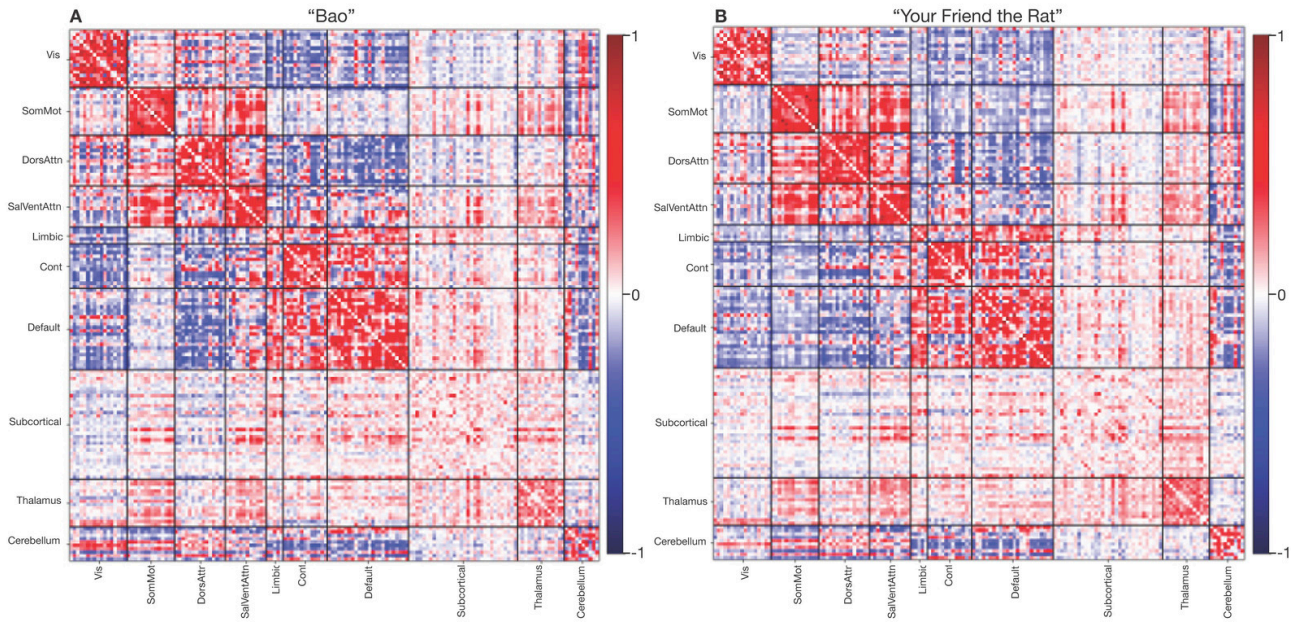

Figure 10. Multi-echo fMRI.

The mean correlation matrices from (**A**) "Bao" and (**B**) "Your Friend the Rat" videos following complete preprocessing are displayed.

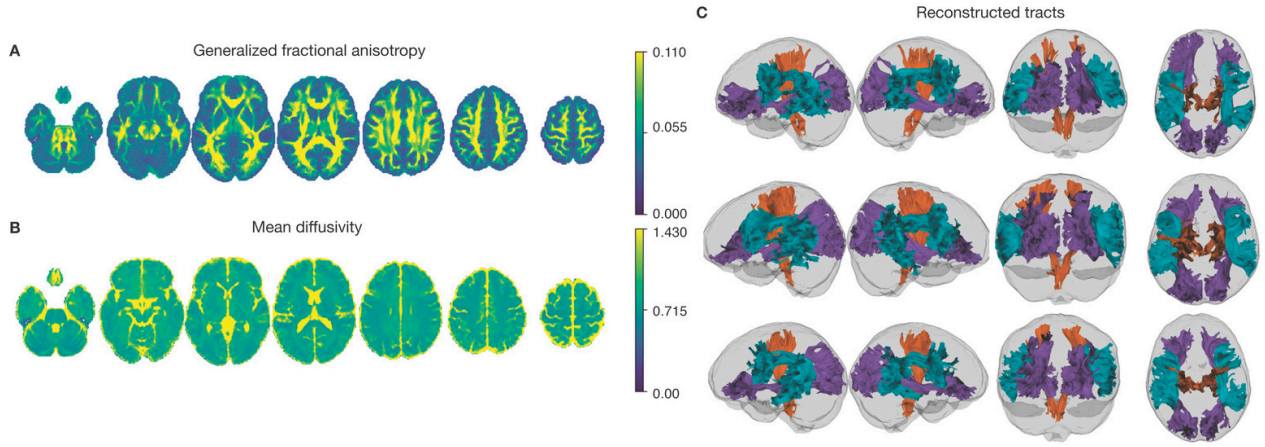

Figure 11. Compressed sensing diffusion spectrum MRI.

Average generalized fractional anisotropy (**A**) and mean diffusivity (**B**) from the initial sample are displayed. Examples of reconstructed white matter tracts from three participants (participants 24683, 24053, and 60295) are displayed in (**C**).

REFERENCES

1. Koenigsberg HW. Affective Instability: Toward an Integration of Neuroscience and Psychological Perspectives. *Journal of Personality Disorders*. 2010;24:60-82. doi:10.1521/pedi.2010.24.1.60

2. Broome MR, He Z, Iftikhar M, Eyden J, Marwaha S. Neurobiological and behavioural studies of affective instability in clinical populations: A systematic review. *Neuroscience & Biobehavioral Reviews*. 2015;51:243-254. doi:10.1016/j.neubiorev.2015.01.021

3. Broome MR, He Z, Iftikhar M, Eyden J, Marwaha S. Neurobiological and behavioural studies of affective instability in clinical populations: A systematic review. *Neuroscience & Biobehavioral Reviews*. 2015;51:243-254. doi:10.1016/j.neubiorev.2015.01.021

4. Koenigsberg HW et al. Are the Interpersonal and Identity Disturbances in the Borderline Personality Disorder Criteria Linked to the Traits of Affective Instability and Impulsivity? *Journal of Personality Disorders*. 2001;15:358-370.

5. Ruch DA et al. Trends in Suicide Among Youth Aged 10 to 19 Years in the United States, 1975 to 2016. *JAMA Netw Open*. 2019;2:e193886. doi:10.1001/jamanetworkopen.2019.3886. PMID:31099867

6. Silvers JA et al. Affective lability and difficulties with regulation are differentially associated with amygdala and prefrontal response in women with Borderline Personality Disorder. *Psychiatry Res*. 2016;254:74-82. doi:10.1016/j.pscychresns.2016.06.009. PMID:27379614

7. Silvers JA et al. Age-Related Differences in Emotional Reactivity, Regulation, and Rejection Sensitivity in Adolescence. *Emotion*. 2012;12:1235-1247. doi:10.1037/a0028297. PMID:22642356

8. Silvers JA, Shu J, Hubbard AD, Weber J, Ochsner KN. Concurrent and lasting effects of emotion regulation on amygdala response in adolescence and young adulthood. *Dev Sci*. 2015;18:771-784. doi:10.1111/desc.12260. PMID:25439326

9. McRae K et al. The development of emotion regulation: an fMRI study of cognitive reappraisal in children, adolescents and young adults. *Soc Cogn Affect Neurosci*. 2012;7:11-22. doi:10.1093/scan/nsr093. PMID:22228751

10. Silvers JA et al. vlPFC–vmPFC–Amygdala Interactions Underlie Age-Related Differences in Cognitive Regulation of Emotion. *Cereb Cortex*. 2017;27:3502-3514.

11. Stephanou K et al. Brain functional correlates of emotion regulation across adolescence and young adulthood. *Hum Brain Mapp*. 2015;37:7-19. doi:10.1002/hbm.22905. PMID:26596970

12. Solmi M et al. Age at onset of mental disorders worldwide: large-scale meta-analysis of 192 epidemiological studies. *Mol Psychiatry*. 2022;27:281-295. doi:10.1038/s41380-021-01161-7. PMID:34079068

13. Marwaha S et al. How is affective instability defined and measured? A systematic review. *Psychol Med*. 2014;44:1793-1808.

14. Gross JJ. The Emerging Field of Emotion Regulation: An Integrative Review. *Review of General Psychology*. 1998;2:271-299. doi:10.1037/1089-2680.2.3.271

15. Williams KE, Chambless DL, Ahrens A. Are emotions frightening? An extension of the fear of fear construct. *Behaviour Research and Therapy*. 1997;35:239-248. doi:10.1016/S0005-7967(96)00098-8

16. Gratz KL, Roemer L. Multidimensional assessment of emotion regulation and dysregulation: Development, factor structure, and initial validation of the difficulties in emotion regulation scale. *Journal of Psychopathology and Behavioral Assessment*. 2004;26:41-54. doi:10.1023/B:JOBA.0000007455.08539.94

17. First MB, Williams JBW, Benjamin LS, Spitzer R. *Structured Clinical Interview for DSM-5® Personality Disorders (SCID-5-PD)*.

18. Stone AA, Shiffman S. Capturing momentary, self-report data: A proposal for reporting guidelines. *ann behav med*. 2002;24:236-243.

19. Lamers F et al. Mood reactivity and affective dynamics in mood and anxiety disorders. *Journal of Abnormal Psychology*. 2018;127:659-669. doi:10.1037/abn0000378

20. Janssen LHC et al. A closer look into the affect dynamics of adolescents with depression and the interactions with their parents: An ecological momentary assessment study. *Eur Child Adolesc Psychiatry*. 2024;33:4259-4272. doi:10.1007/s00787-024-02447-1. PMID:38762682

21. Smith AR et al. The role of anxiety and gender in anticipation and avoidance of naturalistic anxiety-provoking experiences during adolescence: An ecological momentary assessment study. *JCPP Advances*. 2022;2:e12084. doi:10.1002/jcv2.12084. PMID:37431391

22. Trull TJ et al. Affective instability: Measuring a core feature of borderline personality disorder with ecological momentary assessment. *Journal of Abnormal Psychology*. 2008;117:647-661. doi:10.1037/a0012532

23. Santangelo PS et al. The temporal interplay of self-esteem instability and affective instability in borderline personality disorder patients' everyday lives. *Journal of Abnormal Psychology*. 2017;126:1057-1065. doi:10.1037/abn0000288

24. Palmer CA, Oosterhoff B, Bower JL, Kaplow JB, Alfano CA. Associations among adolescent sleep problems, emotion regulation, and affective disorders: Findings from a nationally representative sample. *Journal of Psychiatric Research*. 2018;96:1-8. doi:10.1016/j.jpsychires.2017.09.015

25. Gradisar M et al. Sleep's role in the development and resolution of adolescent depression. *Nat Rev Psychol*. 2022;1:512-523. doi:10.1038/s44159-022-00074-8. PMID:35754789

26. Ritter PS et al. Disturbed sleep as risk factor for the subsequent onset of bipolar disorder – Data from a 10-year prospective-longitudinal study among adolescents and young adults. *Journal of Psychiatric Research*. 2015;68:76-82. doi:10.1016/j.jpsychires.2015.06.005

27. Baum KT et al. Sleep restriction worsens mood and emotion regulation in adolescents. *J Child Psychol Psychiatry*. 2014;55:180-190. doi:10.1111/jcpp.12125. PMID:24889207

28. Goldstone A et al. Sleep Disturbance Predicts Depression Symptoms in Early Adolescence: Initial Findings From the Adolescent Brain Cognitive Development Study. *Journal of Adolescent Health*. 2020;66:567-574. doi:10.1016/j.jadohealth.2019.12.005. PMID:32046896

29. Palmer CA, Alfano CA. Sleep and emotion regulation: An organizing, integrative review. *Sleep Med Rev*. 2017;31:6-16. doi:10.1016/j.smrv.2015.12.006

30. Anastasiades PG, de Vivo L, Bellesi M, Jones MW. Adolescent sleep and the foundations of prefrontal cortical development and dysfunction. *Progress in Neurobiology*. 2022;218:102338. doi:10.1016/j.pneurobio.2022.102338. PMID:35963360

31. Maret S, Faraguna U, Nelson AB, Cirelli C, Tononi G. Sleep and waking modulate spine turnover in the adolescent mouse cortex. *Nat Neurosci*. 2011;14:1418-1420. doi:10.1038/nn.2934. PMID:21983682

32. Tononi G, Cirelli C. Sleep and the Price of Plasticity: From Synaptic and Cellular Homeostasis to Memory Consolidation and Integration. *Neuron*. 2014;81:12-34. doi:10.1016/j.neuron.2013.12.025. PMID:24411729

33. Frank MG. Sleep and Synaptic Plasticity in the Developing and Adult Brain. In: Meerlo P, Benca RM, Abel T, eds. *Sleep, Neuronal Plasticity and Brain Function*. Springer; 2015:123-149. doi:10.1007/7854_2014_305

34. Cheng W et al. Sleep duration, brain structure, and psychiatric and cognitive problems in children. *Mol Psychiatry*. 2021;26:3992-4003. doi:10.1038/s41380-020-0663-2. PMID:32015467

35. Jalbrzikowski M et al. Associations between brain structure and sleep patterns across adolescent development. *Sleep*. 2021;44:zsab120. doi:10.1093/sleep/zsab120. PMID:33971013

36. Hehr A, Huntley ED, Marusak HA. Getting a Good Night's Sleep: Associations Between Sleep Duration and Parent-Reported Sleep Quality on Default Mode Network Connectivity in Youth. *Journal of Adolescent Health*. 2023;72:933-942. doi:10.1016/j.jadohealth.2023.01.010. PMID:36872118

37. Lunsford-Avery JR, Damme KSF, Engelhard MM, Kollins SH, Mittal VA. Sleep/Wake Regularity Associated with Default Mode Network Structure among Healthy Adolescents and Young Adults. *Sci Rep*. 2020;10:509. doi:10.1038/s41598-019-57024-3. PMID:31949189

38. Tashjian SM, Goldenberg D, Monti MM, Galván A. Sleep quality and adolescent default mode network connectivity. *Social Cognitive and Affective Neuroscience*. 2018;13:290-299. doi:10.1093/scan/nsy009. PMID:29432569

39. Krause AJ et al. The sleep-deprived human brain. *Nat Rev Neurosci*. 2017;18:404-418. doi:10.1038/nrn.2017.55. PMID:28515433

40. Souders MC et al. Sleep difficulties related to psychopathology and neurocognition in people with 22q11.2 deletion syndrome. *Psychiatry Res*. 2025;344:116336. doi:10.1016/j.psychres.2024.116336. PMID:39731884

41. Korczak DJ, Madigan S, Colasanto M. Children's Physical Activity and Depression: A Meta-analysis. *Pediatrics*. 2017;139:e20162266. doi:10.1542/peds.2016-2266

42. Fuentealba-Urra S, Rubio A, González-Carrasco M, Oyanedel JC, Céspedes-Carreno C. Mediation effect of emotional self-regulation in the relationship between physical activity and subjective well-being in Chilean adolescents. *Sci Rep*. 2023;13:13386. doi:10.1038/s41598-023-39843-7. PMID:37591897

43. Short MA, Gradisar M, Lack LC, Wright HR, Chatburn A. Estimating adolescent sleep patterns: parent reports versus adolescent self-report surveys, sleep diaries, and actigraphy. *NSS*. 2013;5:23-26. doi:10.2147/NSS.S38369. PMID:23620690

44. de Zambotti M et al. Measures of sleep and cardiac functioning during sleep using a multi-sensory commercially-available wristband in adolescents. *Physiology & Behavior*. 2016;158:143-149. doi:10.1016/j.physbeh.2016.03.006. PMID:26969518

45. Haghayegh S, Khoshnevis S, Smolensky MH, Diller KR, Castriotta RJ. Accuracy of Wristband Fitbit Models in Assessing Sleep: Systematic Review and Meta-Analysis. *Journal of Medical Internet Research*. 2019;21:e16273. doi:10.2196/16273. PMID:31778122

46. Marek S et al. Reproducible brain-wide association studies require thousands of individuals. *Nature*. 2022;603:654-660. doi:10.1038/s41586-022-04492-9. PMID:35296861

47. Gell M et al. How measurement noise limits the accuracy of brain-behaviour predictions. *Nat Commun*. 2024;15:10678. doi:10.1038/s41467-024-54022-6. PMID:39668158

48. Milham MP. Open Neuroscience Solutions for the Connectome-wide Association Era. *Neuron*. 2012;73:214-218. doi:10.1016/j.neuron.2011.11.004

49. Milham MP, Vogelstein J, Xu T. Removing the Reliability Bottleneck in Functional Magnetic Resonance Imaging Research to Achieve Clinical Utility. *JAMA Psychiatry*. 2021;78:587-588. doi:10.1001/jamapsychiatry.2020.4272

50. Laumann TO et al. Functional System and Areal Organization of a Highly Sampled Individual Human Brain. *Neuron*. 2015;87:657-670. doi:10.1016/j.neuron.2015.06.037. PMID:26212711

51. Lee HJ, Dworetsky A, Labora N, Gratton C. Using precision approaches to improve brain-behavior prediction. *Trends in Cognitive Sciences*. 2025;29:170-183. doi:10.1016/j.tics.2024.09.007. PMID:39419740

52. Drysdale AT et al. Resting-state connectivity biomarkers define neurophysiological subtypes of depression. *Nat Med*. 2017;23:28-38. doi:10.1038/nm.4246. PMID:27918562

53. Feczko E et al. The Heterogeneity Problem: Approaches to Identify Psychiatric Subtypes. *Trends in Cognitive Sciences*. 2019;23:584-601. doi:10.1016/j.tics.2019.03.009. PMID:31153774

54. Satterthwaite TD, Feczko E, Kaczkurkin AN, Fair DA. Parsing Psychiatric Heterogeneity Through Common and Unique Circuit-Level Deficits. *Biol Psychiatry*. 2020;88:4-5. doi:10.1016/j.biopsych.2020.04.012. PMID:32553194

55. Lynch CJ et al. Rapid Precision Functional Mapping of Individuals Using Multi-Echo fMRI. *Cell Reports*. 2020;33. doi:10.1016/j.celrep.2020.108540. PMID:33357444

56. Kundu P et al. Multi-echo fMRI: A review of applications in fMRI denoising and analysis of BOLD signals. *Neuroimage*. 2017;154:59-80. doi:10.1016/j.neuroimage.2017.03.033

57. Cieslak M et al. Diffusion MRI head motion correction methods are highly accurate but impacted by denoising and sampling scheme. *Human Brain Mapping*. 2024;45:e26570. doi:10.1002/hbm.26570. PMID:38339908

58. Morris NM, Udry JR. Validation of a self-administered instrument to assess stage of adolescent development. *J Youth Adolescence*. 1980;9:271-280. doi:10.1007/BF02088471

59. Tanner JM. Growth and endocrinology of the adolescent. In: *Endocrine and Diseases of Childhood*. W. B. Saunders; 1969:14-64.

60. Alexander-Bloch A et al. Copy Number Variant Risk Scores Associated With Cognition, Psychopathology, and Brain Structure in Youths in the Philadelphia Neurodevelopmental Cohort. *JAMA Psychiatry*. 2022;79:699-709. doi:10.1001/jamapsychiatry.2022.1017. PMID:35544191

61. Calkins ME et al. The Philadelphia Neurodevelopmental Cohort: constructing a deep phenotyping collaborative. *J Child Psychol Psychiatry*. 2015;56:1356-1369. doi:10.1111/jcpp.12416. PMID:25858255

62. Satterthwaite TD et al. Sex Differences in the Effect of Puberty on Hippocampal Morphology. *J Am Acad Child Adolesc Psychiatry*. 2014;53:341-350.e1. doi:10.1016/j.jaac.2013.12.002. PMID:24565361

63. Sachser C et al. International development and psychometric properties of the Child and Adolescent Trauma Screen (CATS). *J Affect Disord*. 2017;210:189-195. doi:10.1016/j.jad.2016.12.040

64. Mujahid MS, Diez Roux AV, Morenoff JD, Raghunathan T. Assessing the measurement properties of neighborhood scales: from psychometrics to ecometrics. *Am J Epidemiol*. 2007;165:858-867. doi:10.1093/aje/kwm040

65. Centers for Medicare and Medicaid Services, et al. Standardized Screening for Health-Related Social Needs in Clinical Settings: The Accountable Health Communities Screening Tool. *NAM Perspectives*. 2017;7. doi:10.31478/201705b

66. Van Maanen A et al. Screening for Sleep Reduction in Adolescents Through Self-report: Development and Validation of the Sleep Reduction Screening Questionnaire (SRSQ). *Child Youth Care Forum*. 2014;43:607-619. doi:10.1007/s10566-014-9256-z

67. Ghotbi N et al. The µMCTQ: An Ultra-Short Version of the Munich ChronoType Questionnaire. *J Biol Rhythms*. 2020;35:98-110. doi:10.1177/0748730419886986

68. Yu L et al. Development of Short Forms From the PROMISTM Sleep Disturbance and Sleep-Related Impairment Item Banks. *Behavioral Sleep Medicine*. 2012;10:6-24. doi:10.1080/15402002.2012.636266. PMID:22250775

69. Preece DA, Petrova K, Mehta A, Gross JJ. The Emotion Regulation Questionnaire-Short Form (ERQ-S): A 6-item measure of cognitive reappraisal and expressive suppression. *Journal of Affective Disorders*. 2023;340:855-861. doi:10.1016/j.jad.2023.08.076

70. Stringaris A et al. The Affective Reactivity Index: a concise irritability scale for clinical and research settings. *J Child Psychol Psychiatry*. 2012;53:1109-1117. doi:10.1111/j.1469-7610.2012.02561.x. PMID:22574736

71. Alexander LM, Salum GA, Swanson JM, Milham MP. Measuring strengths and weaknesses in dimensional psychiatry. *J Child Psychol Psychiatry*. 2020;61:40-50. doi:10.1111/jcpp.13104. PMID:31423596

72. Pfohl B et al. Reliability and Validity of the Borderline Evaluation of Severity Over Time (Best): A Self-Rated Scale to Measure Severity and Change in Persons With Borderline Personality Disorder. *Journal of Personality Disorders*. 2009;23:281-293. doi:10.1521/pedi.2009.23.3.281. PMID:19538082

73. Carver CS, White TL. Behavioral inhibition, behavioral activation, and affective responses to impending reward and punishment: The BIS/BAS Scales. *Journal of Personality and Social Psychology*. 1994;67:319-333. doi:10.1037/0022-3514.67.2.319

74. Cohen S, Kamarck T, Mermelstein R. A Global Measure of Perceived Stress. *Journal of Health and Social Behavior*. 1983;24:385-396. doi:10.2307/2136404

75. Kroenke K et al. The PHQ-8 as a measure of current depression in the general population. *J Affect Disord*. 2009;114:163-173. doi:10.1016/j.jad.2008.06.026

76. Kroenke K, Spitzer RL. The PHQ-9: A New Depression Diagnostic and Severity Measure. *Psychiatric Annals*. 2002;32:509-515. doi:10.3928/0048-5713-20020901-06

77. Calkins ME et al. Development and Validation of a Brief Age-Normed Screening Tool for Subthreshold Psychosis Symptoms in Youth. *Schizophr Bull sbae224*. Published online 2025. doi:10.1093/schbul/sbae224

78. Zoupou E et al. Validation of the structured interview section of the penn computerized adaptive test for neurocognitive and clinical psychopathology assessment (CAT GOASSESS). *Psychiatry Research*. 2024;335:115862. doi:10.1016/j.psychres.2024.115862. PMID:38554493

79. Gur RC et al. A cognitive neuroscience based computerized battery for efficient measurement of individual differences: Standardization and initial construct validation. *J Neurosci Methods*. 2010;187:254-262. doi:10.1016/j.jneumeth.2009.11.017. PMID:19945485

80. Moore TM, Reise SP, Gur RE, Hakonarson H, Gur RC. Psychometric Properties of the Penn Computerized Neurocognitive Battery. *Neuropsychology*. 2015;29:235-246. doi:10.1037/neu0000093. PMID:25180981

81. Moore TM et al. Construction of a computerized adaptive test (CAT-CCNB) for efficient neurocognitive and clinical psychopathology assessment. *Journal of Neuroscience Methods*. 2023;386:109795. doi:10.1016/j.jneumeth.2023.109795. PMID:36657647

82. Klein A et al. Remote Digital Psychiatry for Mobile Mental Health Assessment and Therapy: MindLogger Platform Development Study. *Journal of Medical Internet Research*. 2021;23:e22369. doi:10.2196/22369. PMID:34762054

83. Granholm E, Loh C, Swendsen J. Feasibility and Validity of Computerized Ecological Momentary Assessment in Schizophrenia. *Schizophrenia Bulletin*. 2007;34:507-514. doi:10.1093/schbul/sbm113. PMID:17932087

84. Larsen RJ, Diener E. Promises and problems with the circumplex model of emotion. In: *Emotion*. Sage Publications, Inc; 1992:25-59.

85. Merikangas KR et al. Real-time Mobile Monitoring of the Dynamic Associations Among Motor Activity, Energy, Mood, and Sleep in Adults With Bipolar Disorder. *JAMA Psychiatry*. 2019;76:190. doi:10.1001/jamapsychiatry.2018.3546. PMID:30540352

86. Mitchell JA et al. Variation in Actigraphy-Estimated Rest-Activity Patterns by Demographic Factors. *Chronobiol Int*. 2017;34:1042-1056. doi:10.1080/07420528.2017.1337032. PMID:28650674

87. Berger AM et al. Methodological Challenges When Using Actigraphy in Research. *J Pain Symptom Manage*. 2008;36:191-199. doi:10.1016/j.jpainsymman.2007.10.008. PMID:18400460

88. Migueles JH, Rowlands AV, Huber F, Sabia S, Hees VT van. GGIR: A Research Community–Driven Open Source R Package for Generating Physical Activity and Sleep Outcomes From Multi-Day Raw Accelerometer Data. Published online 2019. doi:10.1123/jmpb.2018-0063

89. van Hees VT et al. Estimating sleep parameters using an accelerometer without sleep diary. *Sci Rep*. 2018;8:12975. doi:10.1038/s41598-018-31266-z. PMID:30154500

90. Hees VT et al. A Novel, Open Access Method to Assess Sleep Duration Using a Wrist-Worn Accelerometer. *PLOS ONE*. 2015;10:e0142533. doi:10.1371/journal.pone.0142533. PMID:26569414

91. Guo W et al. Processing of Accelerometry Data with GGIR in Motor Activity Research Consortium for Health. *Journal for the Measurement of Physical Behaviour*. 2023;6:37-44. doi:10.1123/jmpb.2022-0018

92. Kang SJ et al. Integrative Modeling of Accelerometry-Derived Sleep, Physical Activity, and Circadian Rhythm Domains With Current or Remitted Major Depression. *JAMA Psychiatry*. 2024;81:911-918. doi:10.1001/jamapsychiatry.2024.1321. PMID:38865117

93. Shafiei G et al. Reproducible Brain Charts: An open data resource for mapping brain development and its associations with mental health. *Neuron*. Published online 2025. doi:10.1016/j.neuron.2025.08.026

94. Casey BJ et al. The Adolescent Brain Cognitive Development (ABCD) study: Imaging acquisition across 21 sites. *Developmental Cognitive Neuroscience*. 2018;32:43-54. doi:10.1016/j.dcn.2018.03.001. PMID:29567376

95. Tisdall MD et al. Volumetric Navigators (vNavs) for Prospective Motion Correction and Selective Reacquisition in Neuroanatomical MRI. *Magn Reson Med*. 2012;68:389-399. doi:10.1002/mrm.23228. PMID:22213578

96. Moser J et al. Multi-echo acquisition and thermal denoising advances precision functional imaging. *Imaging Neuroscience*. 2025;3:imag_a_00426. doi:10.1162/imag_a_00426. PMID:40800744

97. Siegel JS et al. Psilocybin desynchronizes the human brain. *Nature*. 2024;632:131-138. doi:10.1038/s41586-024-07624-5. PMID:39020167

98. Wang J et al. Test–retest reliability of functional connectivity networks during naturalistic fMRI paradigms. *Hum Brain Mapp*. 2017;38:2226-2241. doi:10.1002/hbm.23517. PMID:28094464

99. Gal S, Coldham Y, Tik N, Bernstein-Eliav M, Tavor I. Act natural: Functional connectivity from naturalistic stimuli fMRI outperforms resting-state in predicting brain activity. *NeuroImage*. 2022;258:119359. doi:10.1016/j.neuroimage.2022.119359

100. Simony E, Chang C. Analysis of stimulus-induced brain dynamics during naturalistic paradigms. *NeuroImage*. 2020;216:116461. doi:10.1016/j.neuroimage.2019.116461. PMID:31843711

101. de la Vega A et al. Neuroscout, a unified platform for generalizable and reproducible fMRI research. *eLife*. 2022;11:e79277. doi:10.7554/eLife.79277. PMID:36040302

102. Mahrukh R, Shakil S, Malik AS. Sentiments analysis of fMRI using automatically generated stimuli labels under naturalistic paradigm. *Sci Rep*. 2023;13:7267. doi:10.1038/s41598-023-33734-7. PMID:37142654

103. McNamara Q, De La Vega A, Yarkoni T. Developing a Comprehensive Framework for Multimodal Feature Extraction. In: *Proceedings of the 23rd ACM SIGKDD International Conference on Knowledge Discovery and Data Mining*. ACM; 2017:1567-1574. doi:10.1145/3097983.3098075

104. Vanderwal T, Kelly C, Eilbott J, Mayes LC, Castellanos FX. Inscapes: A movie paradigm to improve compliance in functional magnetic resonance imaging. *NeuroImage*. 2015;122:222-232. doi:10.1016/j.neuroimage.2015.07.069. PMID:26241683

105. Camacho MC et al. Large-scale encoding of emotion concepts becomes increasingly similar between individuals from childhood to adolescence. *Nat Neurosci*. 2023;26:1256-1266. doi:10.1038/s41593-023-01358-9. PMID:37291338

106. Cohen SS, Tottenham N, Baldassano C. Developmental changes in story-evoked responses in the neocortex and hippocampus. *eLife*. 2022;11:e69430. doi:10.7554/eLife.69430. PMID:35787304

107. Vizioli L et al. Lowering the thermal noise barrier in functional brain mapping with magnetic resonance imaging. *Nat Commun*. 2021;12:5181. doi:10.1038/s41467-021-25431-8. PMID:34462435

108. Moeller S et al. NOise reduction with DIstribution Corrected (NORDIC) PCA in dMRI with complex-valued parameter-free locally low-rank processing. *Neuroimage*. 2021;226:117539. doi:10.1016/j.neuroimage.2020.117539. PMID:33186723

109. Van AN et al. Framewise multi-echo distortion correction for superior functional MRI. *bioRxiv*. Published online 2023. doi:10.1101/2023.11.28.568744

110. Wedeen VJ, Hagmann P, Tseng WYI, Reese TG, Weisskoff RM. Mapping complex tissue architecture with diffusion spectrum magnetic resonance imaging. *Magn Reson Med*. 2005;54:1377-1386. doi:10.1002/mrm.20642

111. Daducci A, Van De Ville D, Thiran JP, Wiaux Y. Sparse regularization for fiber ODF reconstruction: From the suboptimality of and priors to. *Medical Image Analysis*. 2014;18:820-833. doi:10.1016/j.media.2014.01.011

112. Maffei C et al. Using diffusion MRI data acquired with ultra-high gradient strength to improve tractography in routine-quality data. *Neuroimage*. 2021;245:118706. doi:10.1016/j.neuroimage.2021.118706. PMID:34780916

113. Yendiki A et al. Post mortem mapping of connectional anatomy for the validation of diffusion MRI. *Neuroimage*. 2022;256:119146. doi:10.1016/j.neuroimage.2022.119146. PMID:35346838

114. Jones R et al. High-fidelity approximation of grid- and shell-based sampling schemes from undersampled DSI using compressed sensing: Post mortem validation. *NeuroImage*. 2021;244:118621. doi:10.1016/j.neuroimage.2021.118621. PMID:34587516

115. Menzel MI et al. Accelerated diffusion spectrum imaging in the human brain using compressed sensing. *Magn Reson Med*. 2011;66:1226-1233. doi:10.1002/mrm.23064

116. Merlet SL, Deriche R. Continuous diffusion signal, EAP and ODF estimation via Compressive Sensing in diffusion MRI. *Med Image Anal*. 2013;17:556-572. doi:10.1016/j.media.2013.02.010

117. Michailovich O, Rathi Y, Dolui S. Spatially regularized compressed sensing for high angular resolution diffusion imaging. *IEEE Trans Med Imaging*. 2011;30:1100-1115. doi:10.1109/TMI.2011.2142189. PMID:21536524

118. Paquette M, Merlet S, Gilbert G, Deriche R, Descoteaux M. Comparison of sampling strategies and sparsifying transforms to improve compressed sensing diffusion spectrum imaging. *Magn Reson Med*. 2015;73:401-416. doi:10.1002/mrm.25093

119. Pu L et al. Model-based compressive diffusion tensor imaging: 2011 8th IEEE International Symposium on Biomedical Imaging: From Nano to Macro, ISBI'11. In: *2011 8th IEEE International Symposium on Biomedical Imaging*. ; 2011:254-257. doi:10.1109/ISBI.2011.5872400

120. Ramirez-Manzanares A, Rivera M, Vemuri BC, Carney P, Mareci T. Diffusion basis functions decomposition for estimating white matter intravoxel fiber geometry. *IEEE Trans Med Imaging*. 2007;26:1091-1102. doi:10.1109/TMI.2007.900461

121. Paquette M, Merlet S, Gilbert G, Deriche R, Descoteaux M. Comparison of sampling strategies and sparsifying transforms to improve compressed sensing diffusion spectrum imaging. *Magn Reson Med*. 2015;73:401-416. doi:10.1002/mrm.25093

122. Zhao L, Vidorreta M, Soman S, Detre JA, Alsop DC. Improving the robustness of pseudo-continuous arterial spin labeling to off-resonance and pulsatile flow velocity. *Magn Reson Med*. 2017;78:1342-1351. doi:10.1002/mrm.26513. PMID:27774656

123. Vidorreta M et al. Whole-brain background-suppressed pCASL MRI with 1D-accelerated 3D RARE Stack-Of-Spirals readout. *PLOS ONE*. 2017;12:e0183762. doi:10.1371/journal.pone.0183762. PMID:28837640

124. Dai W, Robson PM, Shankaranarayanan A, Alsop DC. Reduced resolution transit delay prescan for quantitative continuous arterial spin labeling perfusion imaging. *Magnetic Resonance in Medicine*. 2012;67:1252-1265. doi:10.1002/mrm.23103. PMID:22084006

125. Esteban O et al. fMRIPrep: a robust preprocessing pipeline for functional MRI. *Nat Methods*. 2019;16:111-116. doi:10.1038/s41592-018-0235-4. PMID:30532080

126. Pruim RHR et al. ICA-AROMA: A robust ICA-based strategy for removing motion artifacts from fMRI data. *NeuroImage*. 2015;112:267-277. doi:10.1016/j.neuroimage.2015.02.064

127. DuPre E et al. TE-dependent analysis of multi-echo fMRI with *tedana*. *Journal of Open Source Software*. 2021;6:3669. doi:10.21105/joss.03669

128. Mehta K et al. XCP-D: A Robust Pipeline for the post-processing of fMRI data. *bioRxiv*. Published online 2023. doi:10.1101/2023.11.20.567926

129. Cieslak M et al. QSIPrep: an integrative platform for preprocessing and reconstructing diffusion MRI data. *Nat Methods*. 2021;18:775-778. doi:10.1038/s41592-021-01185-5. PMID:34155395

130. Adebimpe A et al. ASLPrep: a platform for processing of arterial spin labeled MRI and quantification of regional brain perfusion. *Nat Methods*. 2022;19:683-686. doi:10.1038/s41592-022-01458-7. PMID:35689029

131. Gorgolewski K et al. Nipype: a flexible, lightweight and extensible neuroimaging data processing framework in python. *Front Neuroinform*. 2011;5:13.

132. Gorgolewski KJ et al. *Nipype*. Software; 2018. doi:10.5281/zenodo.596855

133. Avants BB, Epstein CL, Grossman M, Gee JC. Symmetric diffeomorphic image registration with cross-correlation: evaluating automated labeling of elderly and neurodegenerative brain. *Med Image Anal*. 2008;12:26-41. doi:10.1016/j.media.2007.06.004. PMID:17659998

134. Tustison NJ et al. N4ITK: improved N3 bias correction. *IEEE Trans Med Imaging*. 2010;29:1310-1320. doi:10.1109/TMI.2010.2046908. PMID:20378467

135. Zhang Y, Brady M, Smith S. Segmentation of brain MR images through a hidden Markov random field model and the expectation-maximization algorithm. *IEEE Trans Med Imaging*. 2001;20:45-57. doi:10.1109/42.906424

136. Dale AM, Fischl B, Sereno MI. Cortical surface-based analysis. I. Segmentation and surface reconstruction. *Neuroimage*. 1999;9:179-194. doi:10.1006/nimg.1998.0395

137. Klein A et al. Mindboggling morphometry of human brains. *PLoS Comput Biol*. 2017;13:e1005350. doi:10.1371/journal.pcbi.1005350. PMID:28231282

138. Ciric R et al. TemplateFlow: FAIR-sharing of multi-scale, multi-species brain models. *Nat Methods*. 2022;19:1568-1571. doi:10.1038/s41592-022-01681-2. PMID:36456786

139. Glasser MF et al. The minimal preprocessing pipelines for the Human Connectome Project. *Neuroimage*. 2013;80:105-124. doi:10.1016/j.neuroimage.2013.04.127. PMID:23668970

140. Marcus DS et al. Informatics and data mining tools and strategies for the human connectome project. *Front Neuroinform*. 2011;5:4. doi:10.3389/fninf.2011.00004. PMID:21743807

141. Esteban O et al. fMRIPrep 24.1.1. *Software*. Published online 2018. doi:10.5281/zenodo.852659

142. Andersson JLR, Skare S, Ashburner J. How to correct susceptibility distortions in spin-echo echo-planar images: application to diffusion tensor imaging. *Neuroimage*. 2003;20:870-888. doi:10.1016/S1053-8119(03)00336-7

143. Jenkinson M, Bannister P, Brady M, Smith S. Improved optimization for the robust and accurate linear registration and motion correction of brain images. *Neuroimage*. 2002;17:825-841. doi:10.1006/nimg.2002.1132

144. Greve DN, Fischl B. Accurate and robust brain image alignment using boundary-based registration. *Neuroimage*. 2009;48:63-72. doi:10.1016/j.neuroimage.2009.06.060. PMID:19573611

145. Pruim RHR, Mennes M, Buitelaar JK, Beckmann CF. Evaluation of ICA-AROMA and alternative strategies for motion artifact removal in resting state fMRI. *NeuroImage*. 2015;112:278-287. doi:10.1016/j.neuroimage.2015.02.063

146. Kundu P et al. Integrated strategy for improving functional connectivity mapping using multiecho fMRI. *Proceedings of the National Academy of Sciences*. 2013;110:16187-16192. doi:10.1073/pnas.1301725110. PMID:24038744

147. Posse S et al. Enhancement of BOLD-contrast sensitivity by single-shot multi-echo functional MR imaging. *Magn Reson Med*. 1999;42:87-97. doi:10.1002/(SICI)1522-2594(199907)42:1

148. van der Walt S, Colbert SC, Varoquaux G. The NumPy Array: A Structure for Efficient Numerical Computation. *Computing in Science & Engineering*. 2011;13:22-30. doi:10.1109/MCSE.2011.37

149. Virtanen P et al. SciPy 1.0: fundamental algorithms for scientific computing in Python. *Nat Methods*. 2020;17:261-272. doi:10.1038/s41592-019-0686-2. PMID:32015543

150. team, T. pandas development. pandas-dev/pandas: Pandas. Published online 2024. doi:10.5281/zenodo.13819579

151. Pedregosa F et al. Scikit-learn: Machine Learning in Python. *Journal of Machine Learning Research*. 2011;12:2825-2830.

152. Abraham A et al. Machine learning for neuroimaging with scikit-learn. *Front Neuroinform*. 2014;8. doi:10.3389/fninf.2014.00014. PMID:24600388

153. Bokeh documentation. Bokeh. https://docs.bokeh.org/en/latest/index.html

154. Hunter JD. Matplotlib: A 2D Graphics Environment. *Computing in Science & Engineering*. 2007;9:90-95. doi:10.1109/MCSE.2007.55

155. Brett M et al. *Nipy/Nibabel: 5.3.1*. Zenodo; 2024. doi:10.5281/zenodo.13936989

156. Ciric R et al. Mitigating head motion artifact in functional connectivity MRI. *Nat Protoc*. 2018;13:2801-2826. doi:10.1038/s41596-018-0065-y. PMID:30446748

157. Satterthwaite TD et al. An improved framework for confound regression and filtering for control of motion artifact in the preprocessing of resting-state functional connectivity data. *Neuroimage*. 2013;64:240-256. doi:10.1016/j.neuroimage.2012.08.052. PMID:22926292

158. Cox RW. AFNI: software for analysis and visualization of functional magnetic resonance neuroimages. *Comput Biomed Res*. 1996;29:162-173. doi:10.1006/cbmr.1996.0014

159. Cox RW, Hyde JS. Software tools for analysis and visualization of fMRI data. *NMR Biomed*. 1997;10:171-178. doi:10.1002/(SICI)1099-1492(199706/08)10:4/5

160. Avants BB, Tustison N, Johnson H. Advanced Normalization Tools (ANTS).

161. Harris CR et al. Array programming with NumPy. *Nature*. 2020;585:357-362. doi:10.1038/s41586-020-2649-2. PMID:32939066

162. Yarkoni T et al. PyBIDS: Python tools for BIDS datasets. *Journal of Open Source Software*. 2019;4:1294. doi:10.21105/joss.01294. PMID:32775955

163. Ciric R et al. Benchmarking of participant-level confound regression strategies for the control of motion artifact in studies of functional connectivity. *NeuroImage*. 2017;154:174-187. doi:10.1016/j.neuroimage.2017.03.020. PMID:28302591

164. Schaefer A et al. Local-Global Parcellation of the Human Cerebral Cortex from Intrinsic Functional Connectivity MRI. *Cereb Cortex*. 2018;28:3095-3114. doi:10.1093/cercor/bhx179. PMID:28981612

165. Pauli WM, Nili AN, Tyszka JM. A high-resolution probabilistic in vivo atlas of human subcortical brain nuclei. *Sci Data*. 2018;5:180063. doi:10.1038/sdata.2018.63. PMID:29664465

166. King M, Hernandez-Castillo CR, Poldrack RA, Ivry RB, Diedrichsen J. Functional boundaries in the human cerebellum revealed by a multi-domain task battery. *Nat Neurosci*. 2019;22:1371-1378. doi:10.1038/s41593-019-0436-x. PMID:31285616

167. Najdenovska E et al. In-vivo probabilistic atlas of human thalamic nuclei based on diffusion- weighted magnetic resonance imaging. *Sci Data*. 2018;5:180270. doi:10.1038/sdata.2018.270. PMID:30480664

168. Glasser MF et al. A multi-modal parcellation of human cerebral cortex. *Nature*. 2016;536:171-178. doi:10.1038/nature18933. PMID:27437579

169. Gordon EM et al. Generation and Evaluation of a Cortical Area Parcellation from Resting-State Correlations. *Cereb Cortex*. 2016;26:288-303. doi:10.1093/cercor/bhu239. PMID:25316338

170. Tian Y, Margulies DS, Breakspear M, Zalesky A. Topographic organization of the human subcortex unveiled with functional connectivity gradients. *Nat Neurosci*. 2020;23:1421-1432. doi:10.1038/s41593-020-00711-6

171. Hermosillo RJM et al. A precision functional atlas of personalized network topography and probabilities. *Nat Neurosci*. 2024;27:1000-1013. doi:10.1038/s41593-024-01596-5. PMID:38532024

172. Zou QH et al. An improved approach to detection of amplitude of low-frequency fluctuation (ALFF) for resting-state fMRI: fractional ALFF. *J Neurosci Methods*. 2008;172:137-141. doi:10.1016/j.jneumeth.2008.04.012. PMID:18501969

173. Jiang L, Zuo XN. Regional Homogeneity: A Multimodal, Multiscale Neuroimaging Marker of the Human Connectome. *Neuroscientist*. 2016;22:486-505. doi:10.1177/1073858415595004. PMID:26170004

174. Zhang B et al. Surface-based regional homogeneity in bipolar disorder: A resting-state fMRI study. *Psychiatry Research*. 2019;278:199-204. doi:10.1016/j.psychres.2019.05.045

175. Taylor PA, Saad ZS. FATCAT: (an efficient) Functional and Tractographic Connectivity Analysis Toolbox. *Brain Connect*. 2013;3:523-535. doi:10.1089/brain.2013.0154. PMID:23980912

176. Garyfallidis E et al. Dipy, a library for the analysis of diffusion MRI data. *Frontiers in neuroinformatics*. 2014;8:8. doi:10.3389/fninf.2014.00008. PMID:24600385

177. Hoopes A, Mora JS, Dalca AV, Fischl B, Hoffmann M. SynthStrip: skull-stripping for any brain image. *NeuroImage*. 2022;260:119474. doi:10.1016/j.neuroimage.2022.119474. PMID:35842095

178. Billot B et al. Robust machine learning segmentation for large-scale analysis of heterogeneous clinical brain MRI datasets. *Proceedings of the National Academy of Sciences*. 2023;120:e2216399120. doi:10.1073/pnas.2216399120. PMID:36802420

179. Veraart J et al. Denoising of diffusion MRI using random matrix theory. *NeuroImage*. 2016;142:394-406. doi:10.1016/j.neuroimage.2016.08.016. PMID:27523449

180. Cordero-Grande L, Christiaens D, Hutter J, Price AN, Hajnal JV. Complex diffusion-weighted image estimation via matrix recovery under general noise models. *Neuroimage*. 2019;200:391-404. doi:10.1016/j.neuroimage.2019.06.039. PMID:31226495

181. Tournier JD et al. MRtrix3: A fast, flexible and open software framework for medical image processing and visualisation. *Neuroimage*. 2019;202:116137.

182. Irfanoglu MO et al. DR-BUDDI (Diffeomorphic Registration for Blip-Up blip-Down Diffusion Imaging) method for correcting echo planar imaging distortions. *Neuroimage*. 2015;106:284-299. doi:10.1016/j.neuroimage.2014.11.042. PMID:25433212

183. Irfanoglu MO, Nayak A, Jenkins J, Pierpaoli C. TORTOISE v3: Improvements and new features of the NIH diffusion MRI processing pipeline. In: *Program and Proceedings of the ISMRM 25th Annual Meeting and Exhibition*. ; 2017.

184. Yeh FC, Wedeen VJ, Tseng WYI. Generalized q-sampling imaging. *IEEE transactions on medical imaging*. 2010;29:1626-1635. doi:10.1109/TMI.2010.2045126

185. Yeh FC. Shape analysis of the human association pathways. *Neuroimage*. 2020;223:117329. doi:10.1016/j.neuroimage.2020.117329. PMID:32882375

186. Adebimpe A et al. ASLPrep . Published online 2023. doi:10.5281/zenodo.3759082

187. Esteban O et al. Analysis of task-based functional MRI data preprocessed with fMRIPrep. *Nature protocols*. 2020;15:2186-2202. doi:10.1038/s41596-020-0327-3. PMID:32514178

188. Lanczos C. Evaluation of Noisy Data. *Journal of the Society for Industrial and Applied Mathematics Series B Numerical Analysis*. 1964;1:76-85. doi:10.1137/0701007

189. Wang Z et al. Empirical optimization of ASL data analysis using an ASL data processing toolbox: ASLtbx. *Magnetic resonance imaging*. 2008;26:261-269. doi:10.1016/j.mri.2007.07.003. PMID:17826940

190. Power JD et al. Methods to detect, characterize, and remove motion artifact in resting state fMRI. *NeuroImage*. 2014;84:320-341. doi:10.1016/j.neuroimage.2013.08.048. PMID:23994314

191. Buxton RB et al. A general kinetic model for quantitative perfusion imaging with arterial spin labeling. *Magn Reson Med*. 1998;40:383-396.

192. Dolui S, Wolf R, Nabavizadeh SA, Wolk DA, Detre JA. Automated Quality Evaluation Index for 2D ASL CBF Maps. International Society for Magnetic Resonance in Medicine. 2016. http://indexsmart.mirasmart.com/ISMRM2017/PDFfiles/0682.html

193. Marwaha S et al. Affective instability, childhood trauma and major affective disorders. *Journal of Affective Disorders*. 2016;190:764-771. doi:10.1016/j.jad.2015.11.024

194. Cole PM, Llera SJ, Pemberton CK. Emotional instability, poor emotional awareness, and the development of borderline personality. *Development and Psychopathology*. 2009;21:1293-1310. doi:10.1017/S0954579409990162

195. Insel T et al. Research Domain Criteria (RDoC): Toward a New Classification Framework for Research on Mental Disorders. *AJP*. 2010;167:748-751. doi:10.1176/appi.ajp.2010.09091379

196. Casey BJ, Oliveri ME, Insel TA. Neurodevelopmental Perspective on the Research Domain Criteria (RDoC) Framework. *Biological Psychiatry*. 2014;76:350-353. doi:10.1016/j.biopsych.2014.01.006

197. Spindler G, Stopsack M, Aldinger M, Grabe HJ, Barnow S. What about the "ups and downs" in our daily life? The influence of affective instability on mental health. *Motiv Emot*. 2016;40:148-161. doi:10.1007/s11031-015-9509-7

198. Marwaha S, Parsons N, Broome M. Mood instability, mental illness and suicidal ideas: results from a household survey. *Soc Psychiatry Psychiatr Epidemiol*. 2013;48:1431-1437. doi:10.1007/s00127-013-0653-7

199. Zuo XN et al. An open science resource for establishing reliability and reproducibility in functional connectomics. *Sci Data*. 2014;1:140049.

200. Xu T et al. ReX: an integrative tool for quantifying and optimizing measurement reliability for the study of individual differences. *Nat Methods*. 2023;20:1025-1028. doi:10.1038/s41592-023-01901-3

201. Kong R et al. Individual-Specific Areal-Level Parcellations Improve Functional Connectivity Prediction of Behavior. *Cerebral Cortex*. 2021;31:4477-4500. doi:10.1093/cercor/bhab101. PMID:33942058

202. Gratton C et al. Functional Brain Networks Are Dominated by Stable Group and Individual Factors, Not Cognitive or Daily Variation. *Neuron*. 2018;98:439-452.e5. doi:10.1016/j.neuron.2018.03.035. PMID:29673485

203. Gordon EM et al. Precision Functional Mapping of Individual Human Brains. *Neuron*. 2017;95:791-807.e7. doi:10.1016/j.neuron.2017.07.011. PMID:28757305

204. Lynch CJ et al. Frontostriatal salience network expansion in individuals in depression. *Nature*. 2024;633:624-633. doi:10.1038/s41586-024-07805-2. PMID:39232159

205. Cui Z et al. Individual Variation in Functional Topography of Association Networks in Youth. *Neuron*. 2020;106:340-353.e8. doi:10.1016/j.neuron.2020.01.029. PMID:32078800

206. Shanmugan S et al. Sex differences in the functional topography of association networks in youth. *Proceedings of the National Academy of Sciences*. 2022;119:e2110416119. doi:10.1073/pnas.2110416119. PMID:35939696

207. Greene DJ et al. Integrative and Network-Specific Connectivity of the Basal Ganglia and Thalamus Defined in Individuals. *Neuron*. 2020;105:742-758.e6. doi:10.1016/j.neuron.2019.11.012. PMID:31836321

208. Rosenberg MD, Finn ES. How to establish robust brain–behavior relationships without thousands of individuals. *Nat Neurosci*. 2022;25:835-837. doi:10.1038/s41593-022-01110-9

209. Ooi LQR et al. Longer scans boost prediction and cut costs in brain-wide association studies. Published online 2024. doi:10.1101/2024.02.16.580448

SUPPLEMENTARY MATERIALS

Supplementary Material

Download: https://apertureneuro.org/article/151820-an-open-fully-processed-data-resource-for-studying-mood-and-sleep-variability-in-the-developing-brain/attachment/320496.docx